

# Sediment Flux and Salt-wedge Dynamics in a Shallow, Stratified Estuary

Author: Kevin J. Simans

Persistent link: <http://hdl.handle.net/2345/bc-ir:108210>

This work is posted on [eScholarship@BC](#),  
Boston College University Libraries.

---

Boston College Electronic Thesis or Dissertation, 2018

Copyright is held by the author, with all rights reserved, unless otherwise noted.

# SEDIMENT FLUX AND SALT-WEDGE DYNAMICS IN A SHALLOW, STRATIFIED ESTUARY

Kevin J. Simans

A thesis

submitted to the Faculty of

the department of Earth and Environmental Sciences

in partial fulfillment

of the requirements for the degree of

Master of Science

Boston College  
Morrissey College of Arts and Sciences  
Graduate School

December 2018

© Copyright 2018 Kevin J. Simans

# **SEDIMENT FLUX AND SALT-WEDGE DYNAMICS IN A SHALLOW, STRATIFIED ESTUARY**

Kevin J. Simans

Advisor: Dr. Gail C. Kineke, Ph.D

An observational study was conducted from 2013 to 2016 to investigate suspended-sediment transport processes in the stratified Connecticut River estuary. Time-series measurements of velocity and suspended-sediment concentration from the upper estuary were analyzed to determine the relative importance of different processes driving sediment flux under highly-variable river discharge. Results indicate that under high discharge the salt intrusion is forced towards the mouth causing large seaward sediment fluxes throughout the water column. Seaward fluxes are dominated by mean advection, with some contribution due to tidal pumping. Under low discharge the salt intrusion extends to the upper estuary, advancing as a bottom salinity front during each flood tide. Stratification and strong velocity shear during the ebb tide cause the upper and lower water column to become dynamically decoupled. Sediment flux near the bed is landward throughout the tidal cycle despite the net seaward depth-integrated flux, and is almost fully attributed to the mean estuarine circulation. River discharge is the primary factor affecting the magnitude and direction of sediment flux because of its high variability and direct connection to the salt-wedge dynamics. A generalized three-phase conceptual model describes suspended-sediment transport in shallow, stratified estuaries with low trapping efficiencies. First, fine sediment bypasses the estuary during high river flows and exports to the coastal ocean where a portion of this sediment is temporarily deposited outside the mouth. Second, during low discharge offshore mud deposits are reworked by

wave- and tidally-driven currents and some sediment is advected back into the estuary with the advancing salt intrusion that transports sediment landward. Third, spatial salinity gradients facilitate sediment transport from the main channel to channel margins, marshes and off-river coves where it is retained and deposited long-term, as demonstrated in prior studies. This re-introduction and trapping of recycled sediment under low-discharge conditions can have important implications for pollutant transport, shoaling of navigation channels and harbors, and salt marsh accretion in the face of rising sea levels.

## TABLE OF CONTENTS

Table of contents.....	v
List of tables.....	vi
List of figures.....	vii
Acknowledgements.....	xi
Introduction.....	1
1.0 Study site.....	5
2.0 Methods.....	7
2.1 Data collection.....	7
2.2 Instrument calibration.....	9
2.3 Sediment flux calculations.....	13
3.0 Results.....	16
3.1 Low discharge – Fall 2013.....	16
3.2 High discharge – Spring 2014.....	18
3.3 Isolated discharge event – Fall 2015.....	20
4.0 Analysis and discussion.....	22
4.1 Total sediment fluxes.....	22
4.2 Cycle of fine sediment transport.....	26
5.0 Summary and conclusions.....	33
6.0 Tables.....	35
7.0 Figures.....	39
8.0 References.....	55

## LIST OF TABLES

1. Summary of relevant quadpod-mounted instruments and data collected during each field deployment.....	35
2. Optical backscatter sensor (OBS) calibrations used in this study to convert raw backscatter (NTU) into SSC (mg/l) using the equation $SSC = a*NTU + b$ . All OBSs record in NTU except for #18507 which records in volts. OBSs were calibrated in the laboratory with Connecticut River sediment.....	36
3. Summary of conditions and results for each field deployment. Positive values of current velocity and sediment flux denote landward transport.....	37
4. Cross-section integrated cumulative sediment fluxes and mean SSCs during each deployment period. Thompsonville and Middle Haddam fluxes were calculated using established rating curves (Woodruff et al. 2013; Yellen et al. 2014), and were taken 27 and 9 hours earlier than the estuary data, respectively, to account for the signal lag between each gauge and the estuary. Estuary fluxes were first calculated from uniform extrapolation of depth-integrated fluxes from the quadpod locations, and were then multiplied by 0.5 based on model results of cross-channel variability (Fig. 12). These fluxes were separated into full water column, lower 30% and upper 70% values. Fall 2013 and Fall 2015 data are from FZ4, and Spring 2014 data are from FZ3. Positive fluxes are in the landward direction. Fluxes from model-guided extrapolation correspond to the values displayed in Figure 13. Estimated uncertainties are included for fluxes at the quadpod locations for each field deployment, and an additional component of uncertainty arises from the lateral extrapolation on the order of 50%.....	38

## LIST OF FIGURES

1. Estuarine parameter space, based on the freshwater Froude number and mixing number. Rectangles indicate the approximate parameter ranges for each estuary due to variations in tidal range, river discharge and bathymetry. The Connecticut River estuary (this study) is indicated by the black box and falls into the time-dependent salt-wedge class under most conditions; mean conditions for the Connecticut are indicated by the black star. SIPS stands for strain-induced periodic stratification. Modified from Figure 6 in Geyer and MacCready (2014).....39
2. a) Location map of the Connecticut River watershed in the northeastern USA with locations of river gauging stations and the estuary shown (TV, Thompsonville; MH, Middle Haddam). b) Connecticut River estuary study site with frontal zones (FZ) and relevant off-river embayments shown. Black diamonds are locations of quadpod deployments in FZ3 (Spring 2014) and FZ4 (Fall 2013 and Fall 2015). Bathymetry data courtesy of Ackerman et al. (2017). c) Bathymetric cross-sections of the estuary at FZ3 and FZ4 showing locations of the quadpods.....40
3. Calibrations for acoustic suspended-sediment data. a) Comparison of SSC derived from calibrated 5 MHz ABS backscatter to gravimetric SSC from colocated pumped water samples from 15 cm above the bed during a tidal cycle in Fall 2015. b) Comparison of SSC derived from calibrated and extrapolated ADCP backscatter to gravimetric SSC from colocated Niskin bottle water samples from ~0.5 m above the bed during a tidal cycle in Spring 2014. c) and d) Comparison of downward-looking 5 MHz ABS to upward-looking 1 MHz ABS at the same heights above the bed in the overlapping region of the two transducers (~0.5-0.9 m above bed) during Fall 2013 (c) and Fall 2015 (d); linear best-fit equations were used to calibrate the upward-looking 1 MHz data. The scatter in all regressions is attributed to different acoustic response to variable suspended-particle characteristics during different phases of the tide and river discharge conditions. Some of the scatter in (b) owes to slight differences in space and time of samples.....41
4. Connecticut River discharge (a) and SSC (b) from 2013 to 2015 including the three field deployments. SSC at Middle Haddam was calculated from an established rating curve (Yellen et al. 2014).....42
5. Mean profiles of velocity and SSC during Fall 2013 (a-b), Spring 2014 (c-d), and Fall 2015 (e-f). Solid bold lines represent mean profiles during times of maximum depth-averaged ebb current, dotted bold lines represent mean profiles during times of maximum depth-averaged flood current, and thin gray lines represent all profiles during maximum ebb and flood current from which the mean profiles were calculated (profiles during only below-mean discharge for Fall 2013 and Fall 2015, and all profiles for Spring 2014). Blue line segments represent extrapolated data. Positive velocities are up-estuary (landward). SSCs during Fall

2013 and Fall 2015 were obtained from calibrated ABS backscatter, and SSCs during Spring 2014 were obtained from calibrated ADCP backscatter. Note the different SSC scales.....43

6. Time-series data collected during the Fall 2013 deployment in FZ4. a) Instantaneous and 88-year daily-mean river discharge at Thompsonville, CT. b) Salinity stratification (difference between bottom and surface salinity) and low-pass filtered (residual) bottom salinity. c) Depth-averaged and residual velocity, with positive values denoting up-estuary (landward) velocities. d) Depth-averaged and residual SSC. Gray shaded regions denote times of spring tides.....44

7. Time series of suspended-sediment fluxes during the Fall 2013 deployment in FZ4. a) Low-pass filtered (residual) total sediment flux integrated over the entire water column and over the lower layer (bottom 30% of the water column). b) Sediment flux decomposed into advective flux and tidal pumping flux, and integrated over the full water column and lower layer. c) Sediment fluxes from panels a-b accumulated over the deployment. Positive fluxes are up-estuary (landward). Gray shaded regions denote times of spring tides.....45

8. Time-series data collected during the Spring 2014 deployment in FZ3. a) Instantaneous and 88-year daily-mean river discharge at Thompsonville, CT. b) Salinity stratification (difference between bottom and surface salinity) and low-pass filtered (residual) bottom salinity. c) Depth-averaged and residual velocity, with positive values denoting up-estuary (landward) velocities. d) Depth-averaged and residual SSC. Gray shaded regions denote times of spring tides.....46

9. Time series of suspended-sediment fluxes during the Spring 2014 deployment in FZ3. a) Low-pass filtered (residual) total sediment flux integrated over the entire water column and over the lower layer (bottom 30% of the water column). b) Sediment flux decomposed into advective flux and tidal pumping flux, and integrated over the full water column and lower layer. c) Sediment fluxes from panels a-b accumulated over the deployment. Positive fluxes are up-estuary (landward). Gray shaded regions denote times of spring tides.....47

10. Time-series data collected during the Fall 2015 deployment in FZ4. a) Instantaneous and 88-year daily-mean river discharge at Thompsonville, CT. b) Salinity stratification (difference between bottom and surface salinity) and low-pass filtered (residual) bottom salinity. c) Depth-averaged and residual velocity, with positive values denoting up-estuary (landward) velocities. d) Depth-averaged and residual SSC. Gray shaded regions denote times of spring tides.....48

11. Time series of suspended-sediment fluxes during the Fall 2015 deployment in FZ4. a) Low-pass filtered (residual) total sediment flux integrated over the entire water column and over the lower layer (bottom 30% of the water column). b) Sediment flux decomposed into advective flux and tidal pumping flux, and integrated over the full water column and lower layer. c) Sediment fluxes from panels a-b

accumulated over the deployment. Positive fluxes are up-estuary (landward).  
Gray shaded regions denote times of spring tides.....49

12. Model results of cross-channel integrated total sediment fluxes during the Fall 2013 (a), Spring 2014 (b) and Fall 2015 (c) deployment periods. Modeled fluxes are obtained from uniform extrapolation of the modeled flux in the thalweg, and from actual modeled fluxes integrated across the estuary. Uniform extrapolation overestimates the total flux by approximately a factor of two. Note the different y-axis scales for each panel.....50

13. Conceptual diagram illustrating total cross-section integrated sediment fluxes during all three field seasons, with Fall 2015 separated into three distinct periods based on changes in river discharge (red box). Black arrows represent fluxes past Middle Haddam in the tidal river (40 km from mouth), green arrows represent fluxes in the upper 70% of the water column in the estuary, and brown arrows represent fluxes in the lower 30% of the water column in the estuary (lower layer). Estuary fluxes during Fall 2013 and Fall 2015 are from FZ4 (9 km from mouth) and fluxes during Spring 2014 are from FZ3 (6 km from mouth). Fluxes correspond to model-guided values reported in Table 4.....51

14. Effects of river discharge on salt intrusion length and sediment flux. a) Cumulative frequency distribution for all discharge data measured at Thompsonville, CT (USGS gauge #01184000) from 1929-2016. The x-axis has been truncated to only include discharge values observed during this study (the largest recorded discharge is 7872 m<sup>3</sup>/s), and only 0.3% of recorded values exceed this range. b) Inverse power-law relationship between discharge and salt intrusion length, defined by the maximum upstream distance where salinity was detected above 2 psu during each tidal cycle, as constrained by the four long-term moored CTDs. c) Relationship between discharge and residual sediment flux in the lower layer from all three field deployments. Landward (positive) fluxes are observed for discharges below ~400 m<sup>3</sup>/s.....52

15. a) Map of the Connecticut River estuary and northeastern Long Island Sound (LIS) showing the percent of fine sediments (>4 φ or <63 μm) at each sampling location. Blue lines are bathymetry, and notable features are labeled. Hamburg Cove grain-size data are from Yellen et al. (2017), estuary data are modified from Valentine (2015) and Lavallee (2017), and LIS data are from this study. b) Mean normalized grain-size distributions of fine sediments from sediment traps inside Hamburg Cove, near-bed suspended samples, mud drape sediment, and bed sediment from the estuary margins, estuary mouth and LIS. All grain-size distributions are unimodal with modes of 4.5 φ for the bed samples and 5.5 φ for the recently-suspended samples. Legend includes the number of individual distributions for each sample type that were averaged. The mud drape distribution (dashed black line) ended with a large value at 10.5 φ which was equally divided over the range 10.5-12 φ.....53

16. Zoom-in of time-series data during low discharge at the beginning of the Fall 2015 deployment in FZ4, illustrating the role of the advancing salt intrusion in transporting sediment landward. a) Water depth and bottom salinity. b) Depth-averaged and near-bed velocity. c) Depth-averaged and near-bed SSC. d) Near-bed suspended-sediment flux. Positive values of velocity and flux are up-estuary (landward). Vertical dashed lines denote the times of peak near-bed SSC during the flood tide (green) and ebb tide (red).....54

## ACKNOWLEDGEMENTS

First I would like to thank my advisor, Dr. Gail Kineke, for her support and guidance throughout the research process. You have taught me a great deal about how to conduct sound science and keep pushing when the going gets tough. Thank you for helping me become the scientist I am today.

I would also like to acknowledge the helpful discussions and advice from my collaborators at Woods Hole Oceanographic Institution, Dr. David Ralston and Dr. Rocky Geyer. Thank you for sharing your knowledge, perspectives and model results to help me tell my story. Also, I thank Jennifer Wehof for her assistance with instrument calibration and helping me understand the complexities of the acoustic backscatter sensor.

I would not be here without the advice, encouragement and reassurance from my thesis committee at Boston College: Dr. Noah Snyder and Dr. Alan Kafka. Thank you for your insight and comments, both on my research and my personal journey through this program. You helped me stay afloat when there were holes in my hull.

Endless thanks are given to my lab group at Boston College: Lisa Kumpf, Katie Lavalley, Kendall Valentine Cole, and Michelle Mullane. Your friendship, teamwork, research ideas and positive attitudes were all incredibly important and I thank you. I cannot imagine having gone through graduate school without you.

Lastly, I want to express the utmost gratitude for the unconditional love and support I received from my girlfriend, Hannah Chambless, and my family. Thank you for always being there as a sounding board and helping me navigate the many curves in the road. I could not have succeeded without you.

This project was funded by National Science Foundation grant OCE-1234164.

## INTRODUCTION

Understanding the dynamics of fine-sediment transport in estuaries continues to be a challenging and important goal in coastal and estuarine research and management, with implications for harbor maintenance and dredging (Simmons and Herrmann 1972), contaminant dispersal and accumulation (Menon et al. 1998; Liu et al. 2011; Geyer and Ralston 2018) and long-term geomorphic evolution of estuarine systems (Patton and Horne 1992; Geyer et al. 2001; Ganju and Schoellhamer 2009). Meade (1969) explained that coastal plain estuaries tend to infill with sediment over time because the estuarine circulation imports sediment from the sea with landward bottom flow. This conclusion was based on the traditional idea of estuarine circulation, where landward flow within the salt intrusion converges with seaward flow near the bed around the upstream limit of salt intrusion (Schubel 1968; Festa and Hansen 1978; Geyer 2010; Burchard et al. 2018).

More recent studies have demonstrated that estuarine sediment flux and particle trapping can be augmented or even dominated by other processes including enhanced settling due to flocculation, frontal trapping, tidal asymmetry and the reduction of vertical turbulent mixing by density stratification. For instance, Milligan et al. (2001) showed that flocculation processes are primarily responsible for rapid deposition and formation of a mobile pool of mud in a dredged channel in South Carolina. A mobile pool has also been documented in the Penobscot River estuary, where large seasonal variations in river discharge cause along-estuary shifts in the locations of salinity fronts and associated sediment remobilization and trapping (Geyer and Ralston 2018). Tidal asymmetry, or flood-ebb differences in current velocity or suspended-sediment concentration (SSC), is generated by semidiurnal variations in mixing and stratification and has been shown to

play a key role in landward sediment transport and trapping in the Columbia River estuary (Jay and Musiak 1994). Scully and Friedrichs (2003) provide an example from the York River estuary where tidal asymmetries in turbulent mixing caused sediment flux to be directed landward even with no residual landward current. Geyer (1993) demonstrated through numerical modeling that stratification may increase the trapping rate of fine sediment in the estuarine turbidity maximum (ETM) by as much as 20 times.

Prior research has established that river discharge exerts a primary influence on the strength of estuarine circulation and the upstream limit of salt intrusion into estuaries, both of which affect sediment flux (Meade 1969; Castaing and Allen 1981; Geyer et al. 2001; Lerczak et al. 2009). An increase in river discharge causes a decrease in the salt intrusion length and a corresponding increase in the longitudinal salinity gradient, resulting in stronger estuarine circulation and more landward bottom flow. Further increases in discharge (i.e. during a freshet) cause a seaward displacement of the limit of salt intrusion and region of landward bottom flow (Meade 1969; Geyer 2010). Sediment fluxes are also affected by fortnightly variations in tidal amplitude causing changes in bed stresses and mixing (Geyer 2010). Tidal amplitude variations can dominate the sediment flux signal in some estuaries such as the Mossoró (Valle-Levinson and Schettini 2016), whereas the combination of spring-neap cycles and discharge variability can result in more complicated sediment transport patterns in other estuaries such as the Hudson (Geyer et al. 2001; Ralston et al. 2012). However, a general feature in stratified estuaries is the occurrence of landward bottom flow in regions where salinity and stratification are present.

Because river discharge and tidal currents can vary markedly between different estuaries and within the same estuary over timescales from days to years, recent research in estuarine dynamics has classified estuaries based on nondimensional parameterizations of these two primary forcing variables in an attempt to draw parallels between estuaries and to predict the estuarine response to changes in forcing (Fig. 1, modified from Geyer and MacCready 2014). The river discharge is parameterized by the freshwater Froude number  $Fr_f = U_R/(\beta g s_{ocean} H)^{1/2}$ , where  $U_R$  is the river outflow velocity (discharge/cross-sectional area),  $\beta \cong 7.7 \times 10^{-4}$ ,  $g$  is gravity,  $s_{ocean}$  is ocean salinity and  $H$  is water depth. The tidal currents are parameterized by the mixing number  $M = [(C_D U_T^2)/(\omega N_0 H^2)]^{1/2}$ , where  $C_D$  is a drag coefficient (typical values around  $3 \times 10^{-3}$ ),  $U_T$  is the depth-averaged tidal current velocity,  $\omega$  is the tidal frequency and  $N_0 = (\beta g s_{ocean}/H)^{1/2}$  is the buoyancy frequency for the maximum vertical salinity difference in an estuary (Geyer and MacCready 2014). Deep, slow-flushing estuaries and fjords fall in the lower left of the parameter space with smallest  $Fr_f$  and  $M$ , partially-mixed estuaries fall in the middle of the diagram, salt-wedge estuaries are at the top, and time-dependent salt-wedge systems are at the top right with largest  $Fr_f$  and  $M$  (Fig. 1). Many early studies of estuarine dynamics and sediment transport have focused on partially- and well-mixed estuaries (e.g. Festa and Hansen 1978; Grabemann and Krause 1989; Geyer et al. 2001), whereas understanding of time-dependent salt-wedge systems has been relatively limited (Geyer and Farmer 1989; Ralston et al. 2010).

The Connecticut River estuary in the northeastern USA is a short, shallow, energetic estuary that falls into the time-dependent salt-wedge class due to its highly-variable river discharge and strong tidal mixing. Coarse sediment (medium sand)

dominates the estuary bed in the main channel, and isolated muddy sediment deposits (fine to medium silt) exist along low-energy margins and in tidal off-river coves and embayments (Woodruff et al. 2013; Valentine 2015). The Connecticut estuary has been described as an inefficient sediment trap that exports 80-90% of suspended sediment and bedload supplied by the river, primarily during high flows (Scatena 1982; Lemieux 1983; Toney 1987; Horne and Patton 1989; Patton and Horne 1992). In the main channel, prevalent seaward-oriented bedforms and a lack of significant bathymetric change over the past century suggest net seaward transport of bedload and no net aggradation, while marginal embayments simultaneously experience rapid deposition of mud (Horne and Patton 1989; Valentine 2015). Long-term accumulation rates of  $>4$  cm/yr have been measured in an embayment (Hamburg Cove) 13 km upstream of the mouth, and dredging records indicate modern accumulation rates of up to 14 cm/yr in an embayment (North Cove) 2.5 km from the mouth (Yellen et al. 2017). Geochemical signatures of Beryllium-7 and Carbon-13 identify the fine sediment trapped in these coves as predominantly marine-derived, suggesting that landward transport within the salt intrusion is the delivery mechanism (Woodruff et al. 2013; Yellen et al. 2017). The import and accumulation of sediment within these coves has been documented, but the larger-scale mechanisms of sediment transport in the river-estuary system have yet to be quantitatively assessed under different discharge conditions and linked to observations in the coves.

The present study aims to quantify the magnitude and direction of sediment flux in a time-dependent salt-wedge estuary under a wide range of discharge conditions and identify the role of the salt-wedge dynamics in transporting sediment landward. To meet

these goals, time-series observations of salinity, velocity and suspended-sediment concentration were collected from the estuary thalweg during high- and low-discharge periods. With these high-resolution measurements, seasonal patterns of flux can be estimated, providing new insight into the conditions necessary for delivering fine sediments to areas of long-term accumulation in the estuary. Further, the results lead to interpretations of sediment transport pathways through the estuary and coastal ocean, and over event to decadal timescales.

## **1.0 STUDY SITE**

The Connecticut River is the longest river on the US east coast, flowing 650 km southward from the Canadian border to Long Island Sound and draining an area of 29,100 km<sup>2</sup> (Fig. 2a). Much of the upper watershed is composed of granitic metamorphic bedrock overlain by erodible glacial tills, whereas the lower river channel is constrained by a crystalline bedrock valley resulting in minimal floodplains and a sandy bed (Horne and Patton 1989). The estuarine morphology is narrow (0.4-1.2 km width) and channelized, and is marked by numerous marginal coves connected to the main stem by tie channels, many of which are artificially deepened by dredging to maintain vessel access (e.g. Hamburg and North Coves; Fig. 2b). Extensive shoals and salt marshes fringe the thalweg close to the river mouth. The western side of the mouth is modified by a jetty and breakwater to protect the dredged navigation channel, whereas on the eastern side the estuary transitions onto a broad shoal that extends 3 to 5 km into Long Island Sound and approximately 10 km alongshore (Patton and Horne 1992).

This study focuses on the region of the lower river that experiences salt intrusion, extending from the river mouth near Old Saybrook, CT to ~15 km upstream (Fig. 2b). Freshwater discharge, as measured 100 km upstream of the mouth and just above the head of tides at Thompsonville, CT (Fig. 2a), ranges from tens to thousands of  $\text{m}^3/\text{s}$  with a long-term mean of  $488 \text{ m}^3/\text{s}$  (88-year record). However, this mean value is exceeded less than one-third of the time and the median discharge is only  $331 \text{ m}^3/\text{s}$  (United States Geological Survey 2015). Low-flow periods are typically observed in late summer, and high flows usually occur during the spring freshet in April and May and isolated storm events that can occur throughout the year (Horne and Patton 1989; Yellen et al. 2014). Salt water penetrates more than 15 km upstream during lowest discharge and is expelled from the estuary during highest flows. The tidal range at the mouth is microtidal at  $1.1 \pm 0.3 \text{ m}$ , and the tidal excursion is comparable to the salt intrusion length, ranging from 6-10 km depending on river flow and tidal conditions. Depth-averaged tidal velocity ( $U_T$ ) during low discharge ranges from 0.3-0.6 m/s with the spring-neap cycle, resulting in values of  $M$  from 1.1 to 2.1. The river outflow velocity ( $U_R$ ) ranges from  $\sim 0.05 \text{ m/s}$  during seasonal low flows to  $\sim 1.0 \text{ m/s}$  during a typical spring freshet, leading to values of  $Fr_f$  from 0.04 to 0.7 (Fig. 1). Thus, the Connecticut River estuary exhibits characteristics of a time-dependent salt-wedge under most conditions, and is partially-mixed during lowest discharges (Garvine 1975; Geyer and MacCready 2014). The dominant forcing is the river discharge due to its high temporal variability and strong influence on the salt-wedge dynamics. In this study, high discharge is considered discharge above the long-term mean and low discharge is below the mean.

Numerous bedrock constrictions in the already-narrow estuarine morphology cause fronts to form in the water column during the ebb tidal phase (Geyer and Ralston 2015; Ralston et al. 2017). These features are characterized by strong, localized along-channel salinity gradients and enhanced stratification, which promote sediment flux convergence and ETM formation. Studies on the complicated dynamics of frontogenesis have shown the importance of fronts to rapid deposition and trapping of fine sediment in the Hudson River estuary (Traykovski et al. 2004; Ralston et al. 2012). In the Connecticut estuary, five frontal zones have been identified and named from FZ1 near the mouth to FZ5 located ~14 km upstream (Ralston et al. 2017). This naming convention is continued in the present study (Fig. 2b).

## **2.0 METHODS**

### **2.1 Data collection**

Field data for this study were collected during three observation periods in Fall 2013, Spring 2014 and Fall 2015. These times were chosen to capture a wide range of discharge conditions. During each four- to five-week observation period, instrumented frames were deployed on the channel bed at multiple locations in the estuary thalweg. Deployment locations were chosen within previously-identified frontal zones where SSCs and trapping rates are enhanced (Fig. 2b; Geyer et al. 2010; Ralston et al. 2017). This study focuses on data collected by acoustic and optical instruments mounted on a 2.5-m-tall quadpod deployed during each field experiment in either FZ3 or FZ4 (Fig. 2b; Fig. 2c). The quadpods provided full-water column profiles of current velocity and acoustic backscatter, and point measurements of salinity and optical backscatter at four

different heights (Table 1). All time-series data were averaged to 20-minute intervals and then 35-hour low-pass filtered to produce tidally-averaged (residual) data.

Supporting datasets come from long-term salinity measurements, shipboard sampling, bed-sediment coring throughout the estuary and outside the mouth, and river discharge and turbidity from stream gauges. Together with the quadpod-mounted CTDs, an array of moored CTDs deployed throughout the estuary provides information on spatial and temporal changes in the along-channel position of the salt intrusion.

Shipboard anchor stations were carried out for a few days during each observation period, including repeated casts with an instrumented profiling tripod (modified after Sternberg et al. 1991) to provide high-resolution measurements through a single tidal cycle. Cross-channel shipboard transects with repeated OBS casts and Niskin bottle samples provide information on the lateral variability of SSC, and serve as another means to ground-truth nearby acoustic-derived SSC measurements.

Extensive bottom-sediment sampling occurred in the estuary from 2012 to 2015 using a KC-Denmark HAPS corer (Valentine 2015). Core locations were repeatedly sampled during successive field campaigns under different discharge conditions, focusing on the frontal zones. Additional sediment sampling took place in June 2017 in Long Island Sound within 7 km of the river mouth and in water depths up to 50 m. Upon recovery, all sediment cores were extruded and two subsamples taken from 0-0.5 cm and 0.5-2 cm depth. In the laboratory, subsamples were processed for grain size by drying, weighing and sieving at 63  $\mu\text{m}$  to determine the mass percent of fine sediments in each sample. The coarse (sand) fractions were sieved at 0.5- $\phi$  intervals and the fine (mud)

fractions were sized using a Micromeritics SediGraph 5120 automated particle size analyzer to produce grain-size distributions (Folk and Ward 1957).

A United States Geological Survey (USGS) gauging station at Thompsonville, CT (#01184000; 100 km from mouth) recorded freshwater discharge from 86% of the watershed as instantaneous (15-minute interval) data and daily-mean values representing the long-term (88-year) mean discharge for each day of the year. This gauge also measured continuous, depth-integrated turbidity starting in 2015. Discrete, depth-averaged SSC measurements at Thompsonville have been used to construct a rating curve between discharge and SSC (Woodruff et al. 2013). Another USGS gauge at Middle Haddam, CT (#01193050; 40 km from mouth) provided continuous near-surface turbidity measurements representative of the tidal river (the region upstream of salinity intrusion but subject to tidal oscillations). Turbidity at Middle Haddam has also been correlated to SSC based on discrete water samples (Yellen et al. 2014).

## 2.2 Instrument calibration

Optical and acoustic instruments were calibrated for SSC using laboratory and field methods. In the laboratory, each OBS was submerged for 30 s in a homogeneous suspension of Connecticut River sediment in a large black bucket to minimize scattering off the bucket sides. Sensors sampled between 1 and 12 Hz, with gain settings that matched those during field deployments. Four concentrations ranging from 0-200 mg/l were used for the calibration. The mean OBS response (NTU) for each concentration was plotted against gravimetrically-determined SSC from filtered water samples, and a linear calibration equation was constructed for each sensor of the form  $SSC = a*NTU + b$ , where  $a$  and  $b$  are the regression coefficients. SSCs from each instrument were calculated

using separate sensor-specific calibrations, all of which had  $r^2 > 0.95$  and  $p < 0.001$  (Table 2).

The theory of acoustic scattering in an aqueous solution of suspended particles has been developed and documented previously (e.g. Thorne et al. 1993; Thorne and Hardcastle 1997), and will be abridged in this thesis. The general principle is that an acoustic transceiver (i.e. a device that both sends and receives a signal) emits a directional pulse of sound, on the order of 10  $\mu\text{s}$  in duration and typically between 0.5-5 MHz in frequency, which propagates through the water column. Sediment or other particles suspended in the water backscatter a proportion of the signal, which is gated into range bins and recorded as a voltage. The intensity of the backscattered signal is related to the concentration, size and shape of suspended particles, and can thus provide information on SSC if particle size and shape are assumed constant in space and time.

The conversion from raw voltage to SSC requires knowledge of certain instrument parameters as well as characteristics of the field sediments where the ABS was deployed. The basic equation relating suspended-sediment concentration,  $C$ , to mean backscattered voltage,  $V_m$ , is as follows:

$$C = \left( \frac{V_m \Psi r}{k_s k_t} \right)^2 e^{4r\alpha} \quad (1)$$

where

$$\Psi = \frac{1 + 1.35 \frac{r}{r_n} + \left( 2.5 \frac{r}{r_n} \right)^{3.2}}{1.35 \frac{r}{r_n} + \left( 2.5 \frac{r}{r_n} \right)^{3.2}} \quad (2)$$

with

$$r_n = \frac{\pi A_t^2}{\lambda} \quad (3)$$

and

$$\alpha = \alpha_w + \alpha_s \quad (4)$$

In the above equations (1) through (4),  $r$  is the range from the transducer (m).  $\Psi$  is the nearfield factor (unitless) that accounts for the departure from spherical acoustic spreading within the transducer nearfield (Downing et al. 1995; Medwin and Clay 1998), and is calculated from the range, transducer radius and frequency.  $r_n$  is the transducer nearfield (m),  $A_t$  is the transducer radius (m), and  $\lambda$  is the wavelength of sound (m) and is equal to the speed of sound in water divided by the transducer frequency.  $k_s$  and  $k_t$  are the sediment backscatter property and system constant, which can be determined through laboratory calibration (discussed below).  $\alpha_w$  is the sound attenuation due to water absorption (Nepers/m), which is determined empirically based on water temperature, salinity, pH and depth (Medwin and Clay 1998).  $\alpha_s$  is the sound attenuation due to suspended-sediment scattering (Nepers/m), which is dependent on SSC. If SSC is relatively low, such as in the Connecticut River estuary (typical SSC maxima <500 mg/l),  $\alpha_s$  is assumed negligible and the inversion follows the above equations with  $\alpha = \alpha_w$ .

Acoustic backscatter sensors were calibrated in a cylindrical recirculating tank (0.3 m diameter, 1.8 m height) in the laboratory following established procedures (Thorne and Hanes 2002; Betteridge et al. 2008; Wehof 2015). A five-minute burst of backscatter data was taken from each ABS in a homogeneous suspension of sediment collected from ~1 m above the bed in the Connecticut River estuary. Ten concentrations were sampled ranging from 0-170 mg/l. Resulting data were corrected for range, nearfield acoustic spreading and water attenuation (Thorne and Hurther 2014), and the corrected mean-square backscattered signal ( $V_c^2$ ) for each transducer was compared with

gravimetrically-determined SSC ( $C$ ). A single calibration constant,  $K$  (equal to  $k_s k_t$ ), was derived from each linear best-fit of  $V_c^2$  vs.  $C$  and incorporated into the conversion of backscatter to SSC (Thorne and Hanes 2002; Thorne and Hurther 2014; Wehof 2015).

An *in situ* verification of the ABS calibration technique was performed during an anchor station during the Fall 2015 field campaign. Acoustic backscatter measurements were compared to SSC determined from filtered water samples obtained throughout a tidal cycle and a linear regression was constructed. Lower-frequency acoustic signals are less sensitive to fine particles, so the 1 MHz underestimated SSC by two orders of magnitude but with moderate correlation ( $r^2 = 0.53$ ). The 5 MHz transducer, more sensitive to fine particles, yielded concentrations much closer to unity with  $r^2$  of 0.61 and root-mean-square error (RMSE) of 34 mg/l (Fig. 3a). The relatively large uncertainty is likely due to flood-ebb differences in the grain-size distribution of suspended particles as a result of flocculation processes (Lavalée 2017), which affects the acoustic calibration by violating the assumption of spatially and temporally invariant size distribution (Thorne and Hurther 2014).

For the Fall 2013 and Fall 2015 time series, the upward-looking 1 MHz signal was correlated to the downward-looking 5 MHz signal within the overlapping region of the two transducers (~0.5 to 0.9 m above bed) and corrected based on the linear best-fit equation for the regression (Fig. 3c, 3d). The uncertainties in these regressions were 5 mg/l and 34 mg/l for Fall 2013 and 2015, respectively. The larger uncertainty during Fall 2015 is attributed to different suspended-particle characteristics during high and low discharge conditions (Lavalée 2017). Full-water column SSC profiles were generated by merging the downward-looking 5 MHz and the corrected upward-looking 1 MHz.

Independent SSC measurements from quadpod-mounted OBSs and shipboard OBS casts generally match the ABS-derived SSCs within a factor of two, with some variability caused by the differential response of acoustic and optical sensors to suspended particles (Lynch et al. 1997).

Instrument malfunction during Spring 2014 rendered the ABS data unusable, and acoustic Doppler current profiler (ADCP) backscatter was used as a proxy for SSC. The ADCP calibration was performed in a similar manner to the ABS (Gartner 2004) and was based on previous ADCP calibrations in the nearby Hudson and Penobscot estuaries (Geyer et al. 2001; Geyer and Ralston 2018). An exponent of -1.2 was used for the range-dependent acoustic decay because that yielded concentrations closest to the ABS during brief periods when ABS data were uncorrupted. The lowest bin of ADCP data was 1.8 m above the bed (mab), necessitating extrapolation of the SSC profiles down to the bed for flux calculations. Extrapolation was attempted using the standard Rouse profile (Rouse 1937), but that resulted in SSCs near the bed being orders of magnitude too high (10s of g/l) compared to other sources of SSC information. Instead, a logarithmic curve was fit to 10 data points in each SSC profile from 4 to 1.8 mab, where SSC usually increases with depth, and each best-fit equation was evaluated from 1.8 mab to the bed. Resulting SSCs agreed well with SSCs from concurrent near-bottom Niskin bottle water samples (RMSE = 17 mg/l), with some of the uncertainty due to slight differences in time and space of the samples (Fig. 3b).

### **2.3 Sediment flux calculations**

Time series of current velocity and SSC were used to compute suspended-sediment fluxes at the thalweg quadpod locations. Current velocities were rotated to the

direction of maximum variance for along-channel velocity. Velocity and SSC data were bin-averaged to 25-cm vertical increments through the entire water column, and each profile was then normalized to relative height above the bed ( $z/h$ ) after accounting for the changing water surface (tides) and bed elevation (erosion and aggradation) during the deployment. The highest ( $z/h = 0.975$ ) and lowest ( $z/h = 0.025$ ) bins were corrupted due to acoustic interference with the water surface and bed, respectively, and were therefore recalculated using extrapolation techniques based on the uncorrupted data in order to obtain best-estimates of depth-integrated sediment fluxes. Velocities in the highest bin were assumed the same as the second-highest bin, and lowest-bin velocities were calculated by taking the mean of the second-lowest bin and zero, assuming the velocity approaches zero at the bed. For the Fall 2013 and Fall 2015 timeseries, lowest-bin SSCs were calculated using a standard Rouse profile fit to the data below the pycnocline. Unlike the ADCP extrapolation described above for the Spring 2014 dataset, the Rouse model yielded reasonable SSC values in the lowest bin at times when SSC was increasing towards the bed. Lowest-bin SSCs were the same as the second-lowest bin when the SSC profile did not fit the Rouse model (i.e. when SSC was not significantly increasing towards the bed). Highest-bin SSCs were assumed the same as those in the second-highest bin.

For each location, instantaneous sediment flux ( $Q_z$ ,  $\text{g/m}^2/\text{s}$ ) at each height above the bed,  $z=z/h$ , was calculated from the product of along-channel velocity ( $u_z$ ) and SSC ( $c_z$ ) using:

$$Q_z = u_z c_z \quad (5)$$

Instantaneous values of  $Q_z$  were vertically integrated through the water column and averaged over the tidal cycle to approximate the total residual along-channel flux per unit width of the estuary,  $Q_T$  (g/m/s). Tidally-averaged (hereafter referred to as residual) values were calculated by applying a 35-hour low-pass filter to the time series of instantaneous, depth-integrated flux.

To quantify the dominant mechanisms affecting sediment flux,  $Q_T$  was decomposed into advective ( $Q_A$ ) and tidal pumping ( $Q_P$ ) components, similar to methods used in past studies (Geyer et al. 2001; Scully and Friedrichs 2007). The advective term represents the flux due to residual-current velocity and residual SSC and is given by

$$Q_A = \bar{u}_z \bar{c}_z \quad (6)$$

where the overbars denote tidally-averaged values. The sediment flux resulting from Stokes drift is contained within  $Q_A$ . The tidal pumping term represents the flux due to correlations between tidal deviations of velocity and SSC and is given by

$$Q_P = u'_z c'_z \quad (7)$$

where the primes indicate temporal deviations from the tidally-averaged values.  $Q_P$  accounts for sediment fluxes caused by both tidal velocity asymmetry and tidal mixing asymmetry.

Uncertainties in calculated sediment fluxes are almost solely due to uncertainties in acoustic-derived SSCs, as acoustic velocities are accurate to within 0.25%. Fractional SSC uncertainties are estimated using the mean SSC values and RMSEs for regressions shown in Figure 3.

### 3.0 RESULTS

High-resolution time series of current velocity and SSC allow calculation of suspended-sediment fluxes at the quadpod locations during each field deployment. Fluxes can then be decomposed to identify the dominant processes using equations (6) and (7). Results are presented separately for each field deployment in order of gauging station data (discharge and SSC), water properties in the estuary (salinity, velocity and SSC) and sediment fluxes (total, decomposed and cumulative). Fluxes are calculated for two zones in order to isolate the effects of landward near-bed transport: integrated over the entire water column, and integrated over only the lower 30% of the water column (hereafter referred to as the “lower layer”;  $z/h = 0.3$ , upper limit of 2.5 to 3 mab). This cutoff depth was chosen because the average depth of zero velocity during maximum ebb tides was at  $z/h=0.3$  during low-discharge conditions. Positive values of velocity and sediment flux denote up-estuary (landward) transport and negative values are down-estuary (seaward). A summary of results from each field deployment is provided in Table 3.

#### 3.1 Low discharge – Fall 2013

The 35-day Fall 2013 deployment was characterized by low discharge, consistently below the daily-mean values and well below the long-term mean (Fig. 4a). A minor discharge event occurred on November 3, 2013 (maximum 640 m<sup>3</sup>/s) and caused a small but noticeable seaward increase of residual velocity and sediment transport in the estuary. SSC data from Thompsonville indicated very low SSCs of 5-10 mg/l in the river at the head of tides. Prior to the Fall 2013 sampling, the 2013 spring freshet was typical of the Connecticut (peak flow = 1700 m<sup>3</sup>/s) and it was followed by several high-

discharge events during the early summer of around 2000 m<sup>3</sup>/s. These events were associated with SSC in the tidal river that exceeded 100 mg/l on multiple occasions (Fig. 4b).

In the estuary at FZ4 (9 km from mouth), mean velocity profiles during ebbs were strongly vertically-sheared, and near-bottom currents remained landward-directed for nearly the entire tidal cycle with magnitudes of 0.1-0.2 m/s (Fig. 5a). SSC around maximum ebb current exhibited higher concentrations throughout the water column than during maximum flood, but the latter increased slightly close to the bottom (Fig. 5b). Salinity stratification (difference between bottom and surface salinity) was tidally-varying and residual bottom salinity was greater than zero throughout the Fall 2013 deployment, indicating the persistent presence of the salt intrusion at FZ4 (Fig. 6b). During neap tides from October 25-30 bottom salinity remained greater than zero at all phases of the tide. Maximum depth-averaged tidal current velocities ranged from 0.20-0.59 m/s during flood tides and 0.23-0.79 m/s during ebbs, with stronger currents observed during periods of spring tides and elevated river discharge (Fig. 6c). Suspended-sediment concentration varied tidally and was greater during spring tides (10-30 mg/l) than during neaps (7-15 mg/l; Fig. 6d). The mean depth-averaged SSC for the entire deployment was only 8 mg/l, similar to SSC measurements at Thompsonville during this period.

Small sediment fluxes on the order of 10 g/m/s were observed during Fall 2013 as a result of low SSC in the upper estuary (Fig. 7a). Fluxes in the lower layer were smaller in magnitude compared with depth-integrated values and were more often landward-directed; average fluxes over the time series were -4.8 g/m/s (depth-integrated) and 2.9

g/m/s (lower layer). Integrating over the deployment period, the cumulative depth-integrated flux over 35 days was -14.6 tonnes per meter of the estuary cross-section (T/m) and the cumulative lower layer flux was 8.7 T/m (Fig. 7c). Decomposition of the total flux reveals that the advective component accounted for 100% of the total depth-integrated flux and 92% of the lower layer flux, pointing to the mean estuarine circulation as the primary mode of sediment transport at FZ4 during Fall 2013. Depth-integrated advective flux was consistently directed seaward due to the net river outflow in the upper water column, whereas in the lower layer this flux was almost always landward as a result of net landward residual near-bed currents (Fig. 7b). Tidal pumping flux was sometimes larger in magnitude than the advective component, yet was relatively unimportant over the length of the timeseries due to landward and seaward pumping fluxes nearly cancelling out.

### **3.2 High discharge – Spring 2014**

Sampling during the 36-day Spring 2014 deployment captured a moderate spring freshet with a maximum river discharge of 2619 m<sup>3</sup>/s occurring at the beginning of the deployment on April 17, 2014 (Fig. 4a; Fig. 8a). The 2014 freshet peak fell into the 62nd percentile of historic spring freshets for the Connecticut and was twice the daily-mean discharge for that date. Suspended-sediment concentration reached a maximum of 126 mg/l at Middle Haddam during the freshet (Fig. 4b). Discharge exceeded the long-term mean for nearly the entire deployment and included two subsequent events with peak discharges of 1574 m<sup>3</sup>/s and 1325 m<sup>3</sup>/s on May 2 and May 19, though SSC in the tidal river remained below 30 mg/l after the initial sediment pulse during highest flow.

High discharge during Spring 2014 had a strong impact on water properties and flow in the estuary. At FZ3 (6 km from mouth) the water column was completely fresh during the first six days of the deployment and again from May 1-5, 2014, despite FZ3 being 3 km closer to the mouth than FZ4 (Fig. 8b). The salt intrusion penetrated landward to FZ3 when discharge dropped below  $\sim 1200 \text{ m}^3/\text{s}$ , as evidenced by the reappearance of residual bottom salinity and tidally-varying stratification (Fig. 8b). Mean profiles during ebbs indicate strong seaward velocities of  $>1 \text{ m/s}$  in the upper water column and  $>0.5 \text{ m/s}$  at 0.4 m above the bed, whereas during flood tides the near-surface flow averaged  $0.10 \text{ m/s}$  seaward and flow was slightly landward near the bed (Fig. 5c). During highest discharge, depth-averaged currents exhibited tidal oscillations in magnitude but flowed in the seaward direction throughout the tidal cycle; only under more moderate discharge conditions were depth-averaged velocities directed landward during flood tides (Fig. 8c). The depth-averaged residual current was seaward for the entire deployment and ranged in magnitude from  $0.22\text{-}1.02 \text{ m/s}$ . Depth-averaged SSC was an order of magnitude greater relative to low-discharge periods in response to the large input of watershed-derived sediment associated with the spring freshet. Mean concentration profiles show higher SSCs during ebb tides ( $25\text{-}250 \text{ mg/l}$ ) compared to flood tides ( $8\text{-}65 \text{ mg/l}$ ; Fig. 5d). Tidal SSC maxima ranged between  $150\text{-}250 \text{ mg/l}$  during highest discharge and  $25\text{-}100 \text{ mg/l}$  during more moderate flows (Fig. 8d).

Large seaward sediment fluxes were observed during Spring 2014 as a result of strong seaward velocities and high SSC. Depth-integrated residual flux was seaward for nearly the entire deployment and peaked at  $-1.14 \text{ kg/m/s}$ , the largest flux observed during this study (Fig. 9a). Largest fluxes occurred when salinity was absent from FZ3 during

the first and second discharge events. The spring-neap cycle exerted a secondary influence on sediment flux, with larger seaward fluxes during spring tides on April 27-30 and smaller fluxes during neaps on May 7-10 when river discharge was similar. This pattern may have been augmented by greater availability of erodible sediment in the estuary during spring tides that occurred just after the first discharge event and large sediment delivery to the estuary. Interestingly, the residual flux integrated over the lower layer remained seaward for nearly all of the Spring 2014 observation period, indicating the dominance of the river outflow even near the bed at FZ3. This is also indicated by the seaward advective flux in the lower layer throughout the time series (Fig. 9b). Tidal pumping fluxes throughout the water column were usually seaward as well, except for a brief period from May 11-15, 2014 when discharge was minimum and small landward pumping fluxes were observed. The cumulative depth-integrated flux over 36 days was -654 T/m, 45 times greater than that observed over a similar time span during Fall 2013 (Fig. 9c). Although the advective term dominated the flux during Spring 2014, tidal pumping played a significant role in the seaward flux at all depths, accounting for 19% of the total. The cumulative flux over the lower layer accounted for over 50% of the depth-integrated flux, as expected based on the mean SSC and velocity profiles.

### **3.3 Isolated discharge event – Fall 2015**

The 28-day Fall 2015 deployment period was dominated by late-season low flows usually below the daily means, with a moderate discharge event (maximum 1096 m<sup>3</sup>/s) from October 1-5, 2015 (Fig. 10a). This isolated event is of particular interest because it occurred suddenly and ended a 70-day period of below-mean discharge. Discharge

increased from 75 m<sup>3</sup>/s to above 1000 m<sup>3</sup>/s in just 1.5 days during the event, while SSC in the tidal river increased from 2 mg/l to nearly 60 mg/l (Fig. 4).

In the upper estuary at FZ4, very low discharge combined with spring tides at the beginning of the deployment resulted in tidally-varying stratification and persistent bottom salinity of 20 psu (Fig. 10b). Depth-averaged currents oscillated tidally with peak magnitudes near 0.5 m/s and the residual velocity was near zero (Fig. 10c). Tidal resuspension of sediment resulted in SSC maxima of 50-150 mg/l and the residual SSC was 25 mg/l during this period. When discharge suddenly increased on October 1, 2015, the limit of salt intrusion shifted seaward to lie in the vicinity of FZ4, as indicated by stratification only occurring briefly during higher-high tides (e.g. October 2 and 3; Fig. 10b). Depth-averaged currents were almost always seaward during the event with magnitudes up to 1 m/s; residual depth-averaged velocity reached a maximum of 0.45 m/s seaward (Fig. 10c). Tidal SSC maxima at FZ4 increased by nearly a factor of two due to enhanced sediment delivery into the estuary (Fig. 10d). During below-mean discharge before and after the event, the mean flow structure was similar to that observed during Fall 2013 including strong velocity shear during ebb tides and weaker, more vertically-uniform velocities during flood tides (Fig. 5e). Mean vertical distributions of SSC during flood tides had low SSCs through most of the water column and a pronounced ten-fold increase in SSC near the bed (Fig. 5f). The mean ebb-tide SSC profile exhibited greater concentrations through most of the water column including a broad mid-water maximum coincident with the height of maximum velocity shear, and no SSC increase near the bed.

Sediment fluxes during Fall 2015 can be divided into two regimes based on discharge. Under low-flow conditions, depth-integrated flux varied tidally and the

residual hovered close to zero (Fig. 11a). In the lower layer, residual flux was very small (5-15 g/m/s) but constantly landward-directed and dominated by advective flux. Conversely, during the discharge event depth-integrated residual flux became strongly seaward reaching a maximum of -0.42 kg/m/s, greater than one-third of the largest flux observed during freshet conditions in Spring 2014 (Fig. 11a). Residual flux in the lower layer during the event followed similar patterns as the full water column but at approximately half the magnitude. Tidal pumping was an important seaward transport mechanism during the discharge event, at times exceeding the advective flux (Fig. 11b). Net landward tidal pumping flux occurred early in the deployment during spring tides and very low discharge, whereas the pumping flux was net seaward for most of the time after the discharge event. The total depth-integrated flux accumulated over 28 days was -81 T/m and the advective flux accounted for 64% of this value. In the lower layer the total cumulative flux was -16.2 T/m, but showed a consistent increasing (landward) trend of about 0.7 T/m/day during periods of low discharge (Fig. 11c). This slow landward flux near the bed was solely due to advective flux, and tidal pumping flux was near zero in the lower layer.

## **4.0 ANALYSIS AND DISCUSSION**

### **4.1 Total sediment fluxes**

One of the goals of this study is to estimate total along-channel fluxes of sediment moving through the Connecticut River estuary by extrapolating the per-unit-width fluxes measured at the mid-channel deployment locations. Using cross-sectional areas of 2620 m<sup>2</sup> at FZ3 and 2520 m<sup>2</sup> at FZ4 and assuming lateral homogeneity, total cumulative fluxes were calculated for each deployment and compared with cumulative fluxes over the same

times at upstream gauging stations (Table 4). However, circulation and SSC can vary markedly across an estuary cross section (Ralston et al. 2012; Valle-Levinson and Schettini 2016), and a more realistic lateral extrapolation of sediment flux was sought that requires information on the cross-channel variability.

Results from a three-dimensional hydrodynamic and sediment transport model developed for the Connecticut River estuary (Ralston et al. 2017) are used to explore the influence of lateral variability and guide flux extrapolations. The 3-D unstructured grid model uses the Finite Volume Coastal Ocean Model (FVCOM; Chen et al. 2003) with a sediment-transport component from the Community Sediment Transport Modeling System (CSTMS; Warner et al. 2008). FVCOM has been used previously to simulate circulation and transport in the stratified Skagit River estuary (Ralston et al. 2013), and has been extensively evaluated against observations in the Connecticut River estuary (Ralston et al. 2017; Yellen et al. 2017).

The model was run for conditions of all three deployment periods. Modeled sediment fluxes from the thalweg integrated uniformly across the estuary are considerably larger in magnitude than modeled laterally-integrated fluxes (Fig. 12). In effect this means that uniform extrapolation of the quadpod data could overestimate total integrated fluxes, assuming the model accurately captures the cross-channel variability. The differences between uniformly-extrapolated and modeled fluxes are smaller (1.5-2x) during high-discharge conditions when seaward transport is likely more uniform across the estuary, whereas these differences are larger (2-4x) during low-discharge conditions when the salt intrusion is present and landward sediment flux is likely confined to the deeper channel. Lateral segregation of sediment flux has been documented in other

estuaries under low-discharge conditions, with net landward transport in the channel and net seaward transport on the shoals (Scully and Friedrichs 2007; Ralston et al. 2012). The existence of a similar lateral structure in the Connecticut estuary would result in an overestimation of landward flux from uniform extrapolation of thalweg fluxes and a larger relative uncertainty than during high-discharge conditions, possibly impacting the interpretations. However, landward fluxes are orders of magnitude smaller than seaward fluxes and have a smaller impact on the cumulative signal despite this larger uncertainty. Therefore, a bulk estimate of 2x is used for the difference between uniformly-extrapolated and modeled fluxes for all discharge conditions, to be applied to the calculation of laterally-integrated total fluxes. The total fluxes presented below carry an estimated uncertainty on the order of 50% associated with lateral variability which augments the uncertainties in acoustic-derived SSCs from the thalweg measurements, so the implications should be interpreted with care. However, observations from the quadpods clearly show landward near-bed flux in the channel during low discharge and seaward flux during high discharge despite the uncertainty in the lateral structure.

Revised estimates of total integrated fluxes are obtained by multiplying by a correction factor of 0.5 to account for the larger fluxes in the thalweg compared to the shoals (Table 4). Total fluxes during the three deployments span three orders of magnitude, with the largest flux during the spring freshet in 2014, intermediate flux during Fall 2015 with an isolated discharge event, and smallest flux during low discharge in Fall 2013 (Fig. 13; Table 4). In general, SSCs and fluxes at Thompsonville are significantly larger than those farther downstream at Middle Haddam (e.g. during Fall 2013 and Spring 2014; Table 4). This counterintuitive result may be a consequence of

imperfect rating curves (Woodruff et al. 2013), but could also result from sediment deposition in the tidal river between the two gauges. Estuary fluxes are similar to those in the tidal river at Middle Haddam during Fall 2013 and Fall 2015, showing a slight increase downstream. The 18% discrepancy during Spring 2014 (140,640 T at Middle Haddam and 115,330 T at FZ3) is attributed to the different method used to obtain SSC in the estuary (from ADCP instead of ABS), which caused a small offset to accumulate over time. For this reason, the flux at FZ3 during Spring 2014 is considered a minimum estimate.

Two key points can be drawn from these findings. First, sediment is transported landward in the lower layer during low discharge even if the total depth-integrated flux is seaward. For instance, during the Fall 2013 deployment about 1,500 tonnes of sediment moved seaward past Middle Haddam and 2,200 tonnes was transported seaward past FZ4 (Fig. 13; Table 4). However, approximately 1,300 tonnes was transported landward in the lower layer due to the influence of the salt intrusion, supplying the upper estuary with sediment available for potential deposition in marshes and off-river coves. This pattern implies a near-bed convergence of sediment flux landward of FZ4, and demonstrates how energetic estuaries can rapidly accumulate fine sediments while simultaneously exporting most of the sediment delivered from upstream.

Second, it appears that prolonged landward transport near the bed leads to the formation of easily-erodible mud deposits upstream of the quadpod locations that are subsequently redistributed downstream during increasing discharge. This process is evidenced by differences between the fluxes at Middle Haddam and FZ4 under different discharge conditions during Fall 2015 (Fig. 13, red box). During low discharge, sediment

is carried seaward past Middle Haddam while landward flux occurs near the bed at FZ4, implying convergence and deposition in the upper estuary and lower tidal river. This occurs because the salt intrusion extends landward of FZ4 when discharge is below the mean, a condition that was met for 70 consecutive days prior to the October 1, 2015 discharge event. During this five-day event, a 46% increase in the seaward flux was observed between Middle Haddam (8,370 T) and FZ4 (12,250 T), indicating that this intervening reach of the river can serve as an additional source of sediment to the estuary when temporary deposits are remobilized during increasing discharge (Fig. 13). These observations support recent work that has emphasized the importance of bed storage in the tidal reach above the limit of salt intrusion in supplying sediment to estuaries (Cook et al. 2007; Sommerfield and Wong 2011). Still, sediment-transport processes in tidal freshwater reaches of rivers represent a significant knowledge gap in the literature, despite the crucial role of the tidal river in modulating sediment delivery to estuaries and the ocean (Ralston and Geyer 2017).

## **4.2 Cycle of fine sediment transport**

The robust time-series observations from this study emphasize the importance of discharge and salt-wedge dynamics in modulating sediment flux in a shallow, stratified estuary. Data from all three field campaigns combine to reveal a strong interrelationship between discharge, salt intrusion length and sediment flux (Fig. 14). Below-mean discharge conditions occur approximately 70% of the time, allowing the salt intrusion to penetrate landward of FZ3 and resulting in small landward sediment fluxes near the bed in the upper estuary. Conversely, less frequent high-discharge conditions restrict the salt intrusion to the lower estuary and cause large seaward sediment fluxes (Fig. 14).

Extrapolating these transport patterns to longer timescales and combining with evidence presented in other studies (Woodruff et al. 2013; Yellen et al. 2017) supports the development of a three-phase conceptual model describing the cycle of fine sediment transport in the Connecticut River estuary that may apply to other dynamically-similar systems: (1) export, (2) import, and (3) deposition and accumulation. This conceptual model does not include processes occurring in the tidal river, except as implied by differences in sediment flux between gauging stations and the estuary.

(1) Export occurs during high flows when sediment is routed through the estuary to Long Island Sound. Much of this sediment is eroded from the upland watershed, but a significant proportion (46% during the Fall 2015 discharge event) is likely remobilized from temporary bed storage in the tidal river and upper estuary. The enhanced discharge restricts the salt intrusion to within a few kilometers of the mouth and large seaward sediment fluxes occur at all depths, sometimes exceeding 1 kg/m/s (Fig. 9; Fig. 14). Fluxes are dominated by non-tidal advection due to the mean river outflow but with some contribution from tidal pumping due to faster currents and greater SSC during ebb tides (Fig. 9). Fine sediment tends to bypass off-river depocenters during high flows (Woodruff et al. 2013; Yellen et al. 2017) and export to the coastal ocean in a buoyant surface plume, where some sediment accumulates near shore on the shallow shoals and the rest is dispersed into the far field by strong tidal currents in Long Island Sound (Garvine 1974). This is consistent with the existence of mud deposits near shore to the west and east of the river mouth, as confirmed by a series of bed-sediment samples collected in June 2017 (Fig. 15a).

(2) Import occurs during low-discharge conditions when sediment is redistributed landward with the advancing salt intrusion. Resuspension of mud deposits by wind- and tidally-driven currents in shallow areas of Long Island Sound makes sediment available for transport into the estuary (Signell et al. 2000; Poppe et al. 2002). During each tidal cycle, import is likely enhanced because flooding currents initiate over the shallow, muddy shoals while the channel flow still ebbs (Scatena 1982; Lemieux 1983). When salt water intrudes during each flood tide, sediment is carried landward with a strong front as indicated by concurrent sharp increases in salinity and SSC, which results in a pulse of landward flux near the bed (Fig. 16; Ralston et al. 2017). The effects of the salt-wedge front passage are also illustrated in mean flood-tide SSC profiles during low discharge, which show SSC increasing near the bed especially during Fall 2015 (Fig. 5b, 5f).

As the tide ebbs, fresh river water is advected over the salt intrusion and stratification usually exceeds 20 psu over only ~8 m depth. Strong vertical gradients of density and velocity result in typical gradient Richardson numbers  $Ri_g = 0.25$  and mixing efficiencies  $Ri_f = 0.23$  within the pycnocline during the mid-ebb (Holleman et al. 2016). Near-surface and near-bed flows are effectively decoupled, which limits vertical turbulent length scales and maintains landward flow and sediment flux near the bed (Scully and Friedrichs 2003). However, the highest SSCs during the ebb occur at mid-depths near the height of maximum velocity shear (Fig. 5f), a likely result of sediment resuspended at the landward limit of the salt-wedge front that advects seaward along the pycnocline. As the tide progresses to late ebb, the salt-wedge structure is advected downstream causing a decrease in stratification and corresponding decreases in  $Ri_g$  and  $Ri_f$  during the transition from internal shear layer mixing to bottom boundary layer

mixing (Holleman et al. 2016; Ralston et al. 2017). Once stratification disappears, turbulence can reach the bed and resuspend sediment resulting in a smaller secondary peak in near-bed SSC (Fig. 16c).

The depth-integrated flux is slightly seaward during low discharge (although 2 to 3 orders of magnitude smaller than during high discharge) due to mixing of sediment higher in the water column during the ebb, but the near-bed currents usually remain landward even during maximum depth-averaged ebb current and this drives a landward advective flux within the lower layer. Thus, fine sediment is pumped back and forth with each tide but the tidally-averaged motion is landward near the bed, so sediment slowly makes its way up the estuary (Wellershaus 1981; Geyer 1993).

This re-import of marine-sourced sediment is also evidenced by trends in bed composition revealed by extensive sediment sampling throughout the study area (Fig. 15). In addition to deposits along the channel margins and outside the mouth, fine sediments occur as a “mud drape” (1-mm-thick ephemeral mud layer on top of sand) that is only observed in the main channel of the upper estuary during low-discharge periods when the salt intrusion is present (Valentine 2015). Mean grain-size distributions of the fine fractions ( $<63 \mu\text{m}$ ) were obtained by averaging many individual distributions for six different types of sediment samples: Hamburg Cove sediment traps (Yellen et al. 2017), mud drape samples (Valentine 2015), near-bed suspended disaggregated inorganic grain size (DIGS; Lavallee 2017), estuary margins, estuary mouth and Long Island Sound (Fig. 15b). All distributions are unimodal, with modes of  $4.5 \phi$  ( $44 \mu\text{m}$ ) for the bed samples (margins, mouth, LIS) and  $5.5 \phi$  ( $22 \mu\text{m}$ ) for the recently-suspended samples (Hamburg Cove, mud drape, DIGS). The distribution of the fine sediment deposited at and beyond

the estuary mouth is nearly the same as that being transported and deposited throughout the study area, providing further evidence that fine sediment exported to Long Island Sound is subsequently re-imported into the estuary.

(3) Deposition and accumulation occur simultaneously with the import phase during low-discharge conditions, and involve the transport of suspended sediment from the main estuary channel into depositional environments such as channel margins, off-river coves and marshes. Sediment tends to bypass such environments during high river flows when salinity is absent, and accumulates during low flows when salinity intrudes and creates density gradients between the main channel and off-river environments (Woodruff et al. 2013; Yellen et al. 2017). Previous work in Hamburg Cove has shown that saline water and suspended sediment can flow as a dense gravity current through the dredged cove entrance and into deeper areas of the cove during flood tides, but only when the pycnocline in the main channel rises above the depth of the cove entrance (i.e. when the salt-intrusion front reaches the entrance). Fine sediment transported into the cove tends to become trapped there because stratification causes stagnation of bottom water and limits resuspension during the ensuing ebb tide (Yellen et al. 2017). The mean size distribution of Hamburg Cove fine sediments is slightly finer than distributions from bed deposits throughout the estuary and Long Island Sound, indicating that the finer mud particles are preferentially delivered to the cove (Fig. 15b).

Time-series observations from FZ4 under low-discharge conditions show that the highest SSCs occur near the bed during each flood tide and are coincident with the passage of the salt front, driving an up-estuary flux (Fig. 16). Thus, favorable conditions for sediment transport into marginal environments occur during each flood tide because

seaward-sourced sediment is delivered to the upper estuary synchronous with enhanced salinity gradients. The salt intrusion reaches the Hamburg Cove entrance when discharge is below  $\sim 300 \text{ m}^3/\text{s}$ , which occurs during half of the year on average (Fig. 14b). At more seaward embayments such as North Cove (Fig. 2b), salt is present at all but the highest discharges and consequently sediment accumulation rates there are much greater than in coves farther up-estuary (Yellen et al. 2017).

It stands to reason that marginal embayments and salt marshes that lie within the typical salt intrusion length can serve as sediment traps in estuaries that may otherwise have low trapping efficiencies in the main channel. This is especially true for harbors with dredged channels, such as North Cove and Hamburg Cove, that more easily exchange water and sediment with the main channel due to the increased water depth. The sediment-trapping mechanism is absent from the estuary when most sediment is being delivered from the watershed during high flows, but is present during low flows when the salt intrusion is established. Although landward fluxes during low discharge are small in magnitude, they occur over a majority of the time and are important for supplying fine sediment to the estuary to maintain marshes and equilibrium morphology in the face of rising global sea levels. Marshes can degrade or disappear if the rate of sea level rise outpaces marsh accretion rates, which depend on SSC and sediment delivery (Temmerman et al. 2004). Furthermore, increases in mean sea level can increase the salt intrusion length into estuaries, likely causing changes in the positions of ETM and associated zones of enhanced sediment trapping (Hong and Shen 2012; Yellen et al. 2017). Thus, understanding estuarine sediment flux and deposition combined with salt-

wedge dynamics under a range of forcing conditions is a vital step in predicting future changes to estuarine morphology (Ganju and Schoellhamer 2009).

## 5.0 SUMMARY AND CONCLUSIONS

This research provides a basis for understanding the transport mechanisms and fate of fine sediment in energetic estuaries with low trapping efficiencies, such as the Connecticut River estuary. As is the case for many field studies of sediment transport, the quantitative fluxes presented here are subject to large uncertainties stemming from challenges of instrument calibration (Fig. 3) and data extrapolation (Table 4) and should be taken as broad estimates, but the conclusions are backed by several different lines of evidence and are considered robust. River discharge exerts a leading-order influence on the magnitude and net direction of sediment transport, causing large seaward fluxes at all depths during high discharge and small bi-directional fluxes with seaward flux in the upper water column and landward flux near the bed during low discharge (Fig. 13; Fig. 14). The advective flux dominates under most conditions indicating persistent estuarine circulation, with a notable component of seaward tidal pumping flux during high discharge due to stronger currents and greater SSC during ebb tides (Fig. 9; Fig. 11).

The combined evidence from this study and others (Woodruff et al. 2013; Yellen et al. 2017) suggests a conceptual model for fine sediment transport in this system that may be applicable to other shallow, tidal, stratified estuaries with variable discharge forcing. Over seasonal to inter-annual timescales, sediment is flushed out of the estuary during high discharge and some is deposited offshore near the mouth (1), providing a source of sediment to the estuary during low discharge when the tidal salt intrusion re-establishes. Sediment is then transported slowly up-estuary towards the limit of salt intrusion (2) where it can be transmitted into marginal environments and permanently deposited (3). Fine sediment can accumulate rapidly in energetic estuaries with primarily

sandy beds, but requires this multi-step transport pathway. However, transport processes within the tidal freshwater reach are inferred from differences between total integrated fluxes which carry large uncertainties, and should be interpreted with care. Tidal river dynamics can significantly affect sediment fluxes in the estuary (e.g. Ralston and Geyer 2017), and represent a knowledge gap in the complete cycle of estuarine sediment transport. Future studies should include more detailed attention to this issue.

## 6.0 TABLES

**Table 1.** Summary of relevant quadpod-mounted instruments and data collected during each field deployment.

<b>Instrument</b>	<b>Manufacturer</b>	<b>Data provided</b>	<b>Sampling interval</b>	<b>Data range (meters above bed/below surface)</b>
Acoustic Doppler current profiler (ADCP)	Teledyne RD	Profiles of current velocity and acoustic backscatter	30 s	Upward: 1.5 mab - surface
Aquadopp	Nortek	Profiles of near-bed current velocity	60 s	Downward: 1.3 mab - bed
AQUAScat 1000 Acoustic backscatter sensor (ABS)	Aquatec LTD	Profiles of acoustic backscatter	2 s, 5- to 20-min bursts	Upward (1 MHz): 0.3 mab - surface Downward (1, 2.5, 5 MHz): 1.0 mab – bed
Conductivity, temperature and depth sensor (CTD) with attached optical backscatter sensor (OBS)	RBR, Seapoint	Point measurements of salinity and optical backscatter	30 s	Bottom: 0.5 mab Middle: 1.2 mab Upper: 2.2 mab Surface: 0.6 mbs

**Table 2.** Optical backscatter sensor (OBS) calibrations used in this study to convert raw backscatter (NTU) into SSC (mg/l) using the equation  $SSC = a*NTU + b$ . All OBSs record in NTU except for #18507 which records in volts. OBSs were calibrated in the laboratory with Connecticut River sediment.

<b>OBS serial #</b>	<b><i>a</i></b>	<b><i>b</i></b>	<b><math>r^2</math></b>	<b>RMSE (mg/l)</b>
14639	2.15	-3.28	0.998	3.20
14640	2.61	-1.79	0.999	1.12
17140	1.96	-4.84	0.998	3.62
17211	1.00	-12.83	0.946	17.30
17212	1.81	6.65	0.999	1.40
18503	2.31	-1.19	0.999	0.88
65524	2.13	-6.94	1.000	0.42
65525	2.48	-2.49	0.999	0.74
65526	2.07	-2.91	0.999	0.80
65640	1.68	-0.97	0.999	0.86
65722	1.83	-1.44	0.999	1.03
65723	1.79	-0.80	0.999	1.31
18658	1.70	-0.44	0.999	0.89
18507	48.03	2.56	0.999	1.77

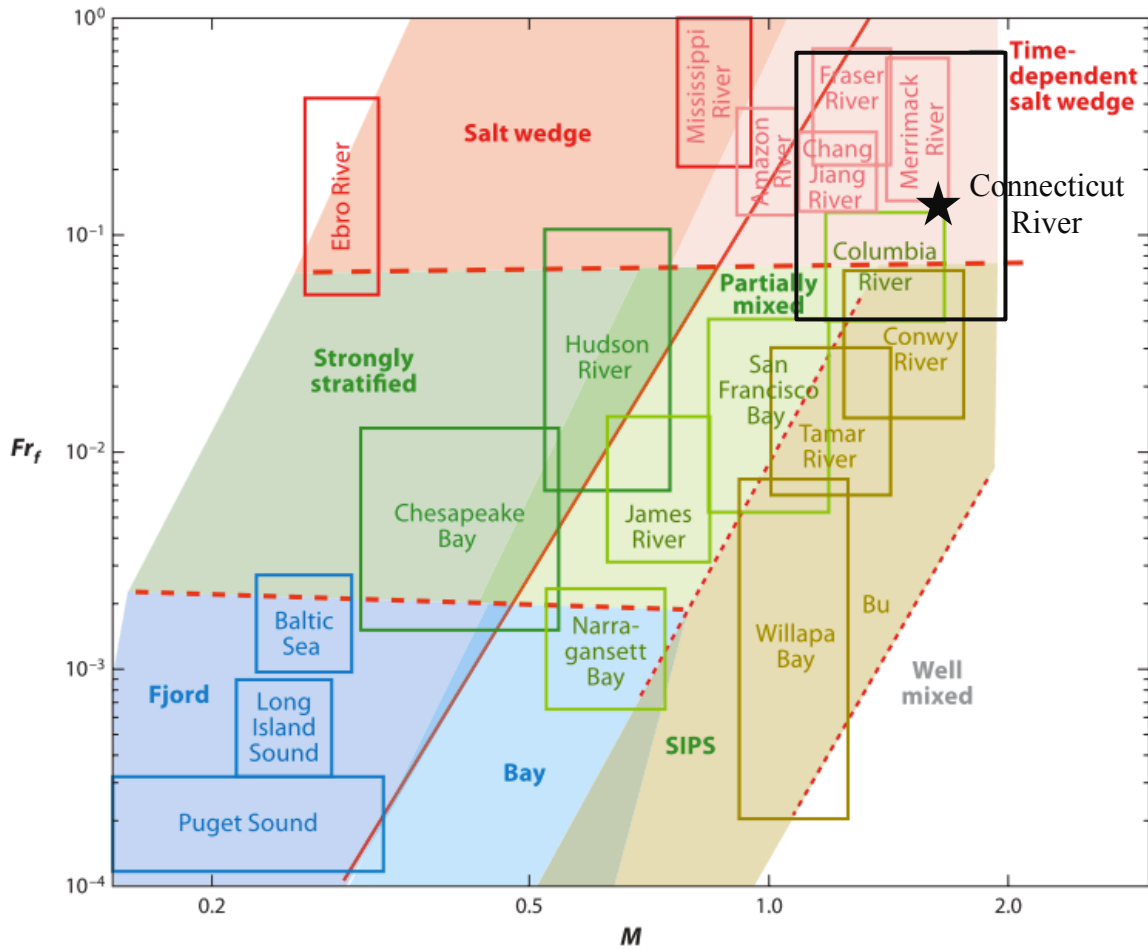
**Table 3.** Summary of conditions and results for each field deployment. Positive values of current velocity and sediment flux denote landward transport.

	<b>Fall 2013</b>	<b>Spring 2014</b>	<b>Fall 2015</b>
<b>Deployment length (days)</b>	35	36.5	28.5
<b>Quadpod location (coordinates)</b>	FZ4 (41°20.364'N, 72°21.689'W)	FZ3 (41°18.966'N, 72°20.749'W)	FZ4 (41°20.369'N, 72°21.681'W)
<b>Min discharge (m<sup>3</sup>/s)</b>	89	462	75
<b>Mean discharge (m<sup>3</sup>/s)</b>	243	1109	295
<b>Max discharge (m<sup>3</sup>/s)</b>	640	2619	1096
<b>Mean tidal range (m)</b>	1.1	1.0	1.1
<b>Max depth-averaged flood velocity (m/s)</b>	0.59	0.46	0.61
<b>Max depth-averaged ebb velocity (m/s)</b>	-0.79	-1.3	-0.96
<b>Mean depth-averaged SSC (mg/l)</b>	8	41	21
<b>Max depth-averaged SSC (mg/l)</b>	117	244	264
<b>Mean depth-integrated total flux (kg/m/s)</b>	-0.0048	-0.21	-0.034
<b>Max depth-integrated total flux (kg/m/s)</b>	-0.031	-1.1	-0.42
<b>Cumulative depth-integrated total flux (tonne/m)</b>	-14.6	-654	-80.9
<b>Cumulative lower layer total flux (tonne/m)</b>	8.7	-345	-16.2

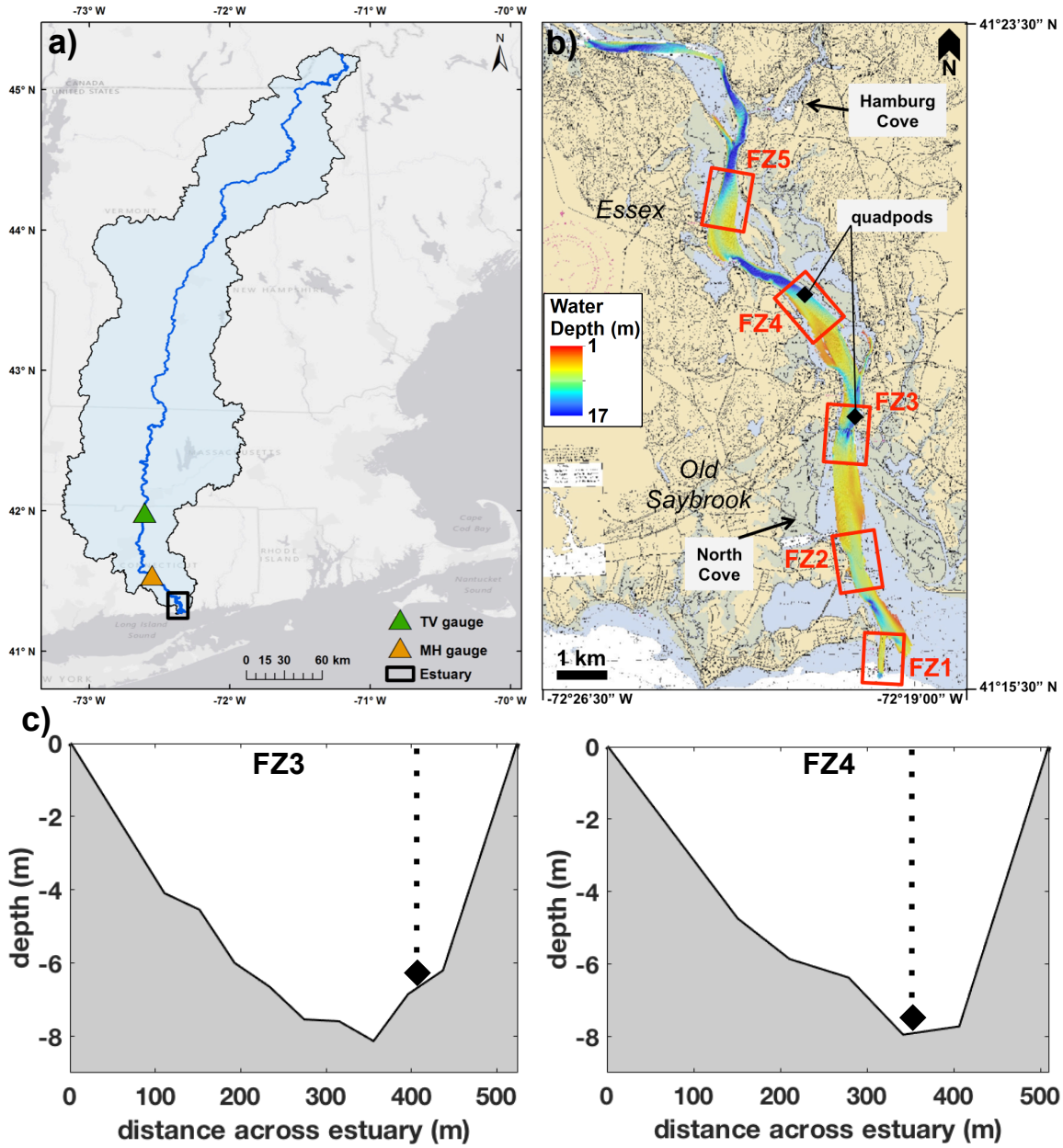
**Table 4.** Cross-section integrated cumulative sediment fluxes and mean SSCs during each deployment period. Thompsonville and Middle Haddam fluxes were calculated using established rating curves (Woodruff et al. 2013; Yellen et al. 2014), and were taken 27 and 9 hours earlier than the estuary data, respectively, to account for the signal lag between each gauge and the estuary. Estuary fluxes were first calculated from uniform extrapolation of depth-integrated fluxes from the quadpod locations, and were then multiplied by 0.5 based on model results of cross-channel variability (Fig. 12). These fluxes were separated into full water column, lower 30% and upper 70% values. Fall 2013 and Fall 2015 data are from FZ4, and Spring 2014 data are from FZ3. Positive fluxes are in the landward direction. Fluxes from model-guided extrapolation correspond to the values displayed in Figure 13. Estimated uncertainties are included for fluxes at the quadpod locations for each field deployment, and an additional component of uncertainty arises from the lateral extrapolation on the order of 50%.

<b>Deployment (length)</b>	<b>Fall 2013 (35 d)</b>	<b>Spring 2014 (36.5 d)</b>	<b>Fall 2015 (28.5 d)</b>
<b>Cumulative flux at Thompsonville (tonnes)</b>	-4,660	-207,300	-9,410
<b>Cumulative flux at Middle Haddam (tonnes)</b>	-1,510	-140,640	-9,540
<b>Cumulative flux at estuary, uniform extrapolation (tonnes)</b>	<b>Upper 70%:</b> -7,040	-108,860	-19,980
	<b>Lower 30%:</b> 2,620	-121,800	-5,020
	<b>Full:</b> -4,420	-230,660	-25,000
<b>Cumulative flux at estuary, model-guided extrapolation (tonnes)</b>	<b>Upper 70%:</b> -3,520	-54,430	-9,990
	<b>Lower 30%:</b> 1,310	-60,900	-2,510
	<b>Full:</b> -2,210	-115,330	-12,500
<b>Estimated uncertainty in thalweg fluxes (%)</b>	66	118	66
<b>Mean SSC at Thompsonville (mg/l)</b>	6	40	8
<b>Mean SSC at Middle Haddam (mg/l)</b>	2	24	6
<b>Mean SSC at estuary (mg/l)</b>	8	41	21

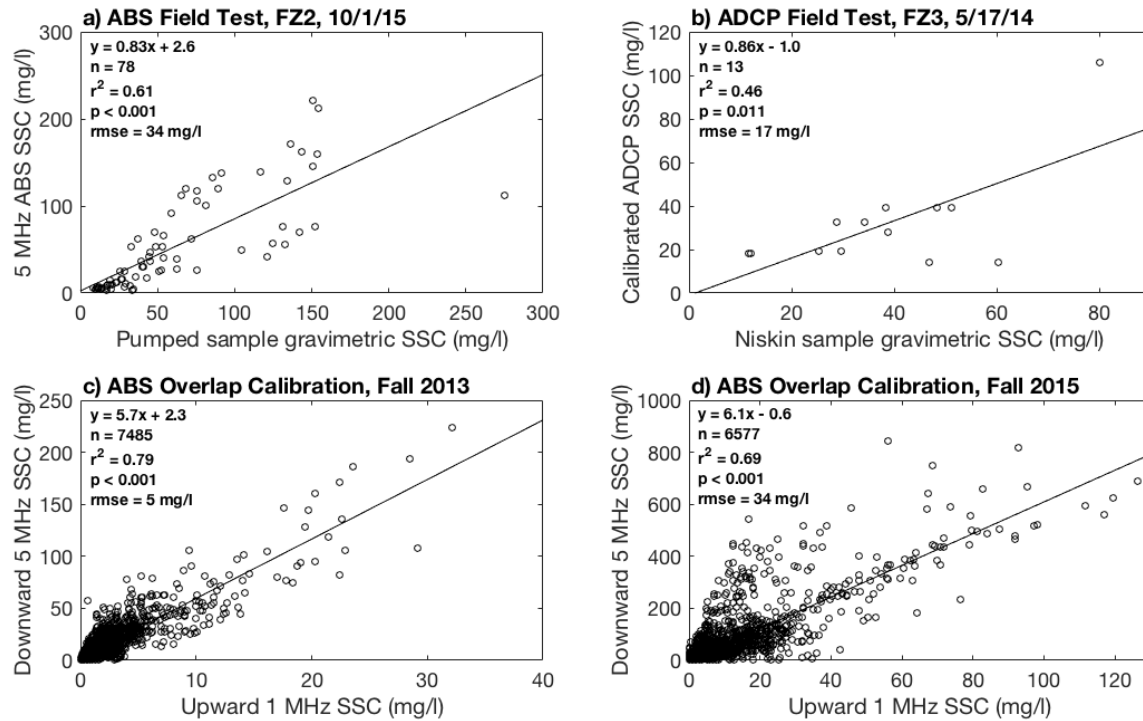
## 7.0 FIGURES



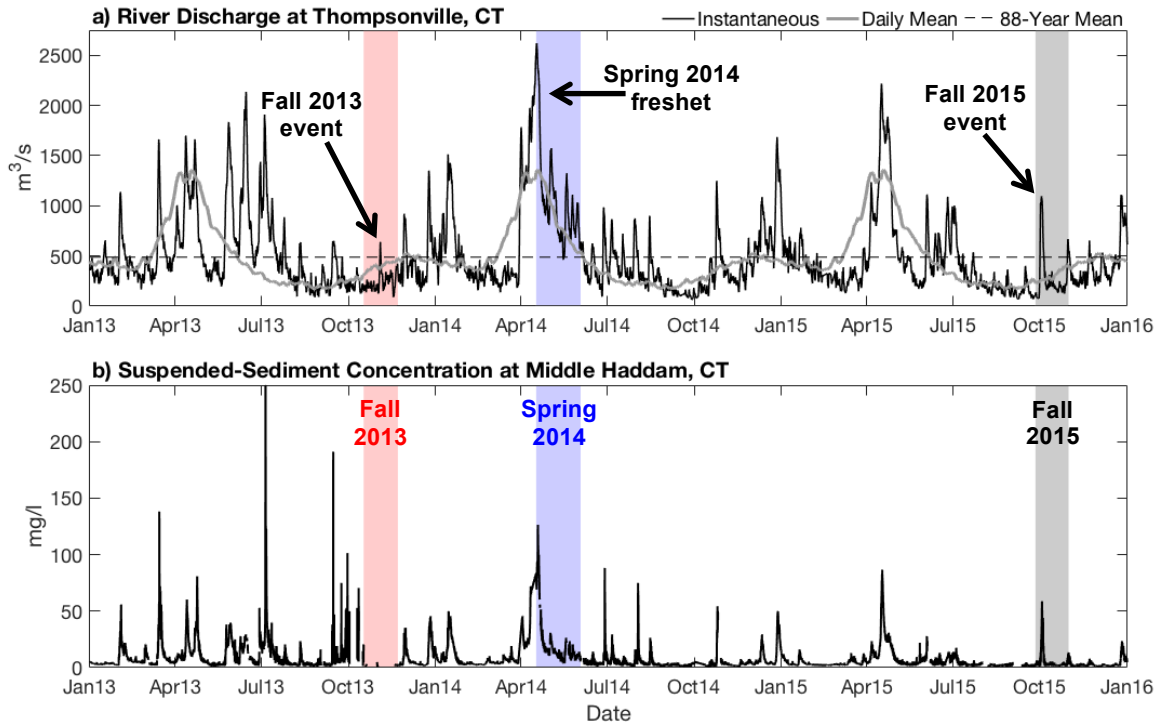
**Figure 1.** Estuarine parameter space, based on the freshwater Froude number and mixing number. Rectangles indicate the approximate parameter ranges for each estuary due to variations in tidal range, river discharge and bathymetry. The Connecticut River estuary (this study) is indicated by the black box and falls into the time-dependent salt-wedge class under most conditions; mean conditions for the Connecticut are indicated by the black star. SIPS stands for strain-induced periodic stratification. Modified from Figure 6 in Geyer and MacCready (2014).



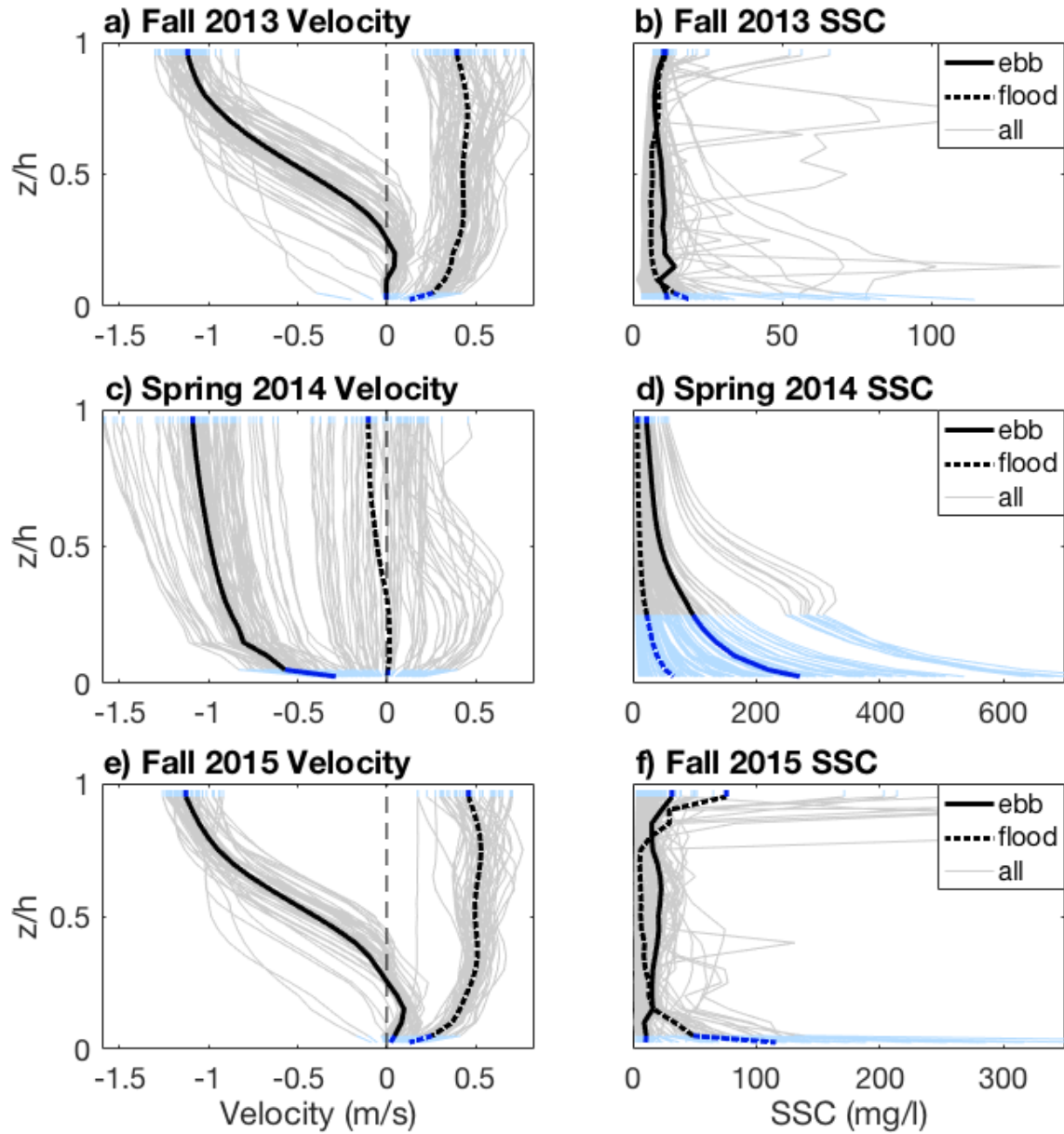
**Figure 2.** a) Location map of the Connecticut River watershed in the northeastern USA with locations of river gauging stations and the estuary shown (TV, Thompsonville; MH, Middle Haddam). b) Connecticut River estuary study site with frontal zones (FZ) and relevant off-river embayments shown. Black diamonds are locations of quadpod deployments in FZ3 (Spring 2014) and FZ4 (Fall 2013 and Fall 2015). Bathymetry data courtesy of Ackerman et al. (2017). c) Bathymetric cross-sections of the estuary at FZ3 and FZ4 showing locations of the quadpods.



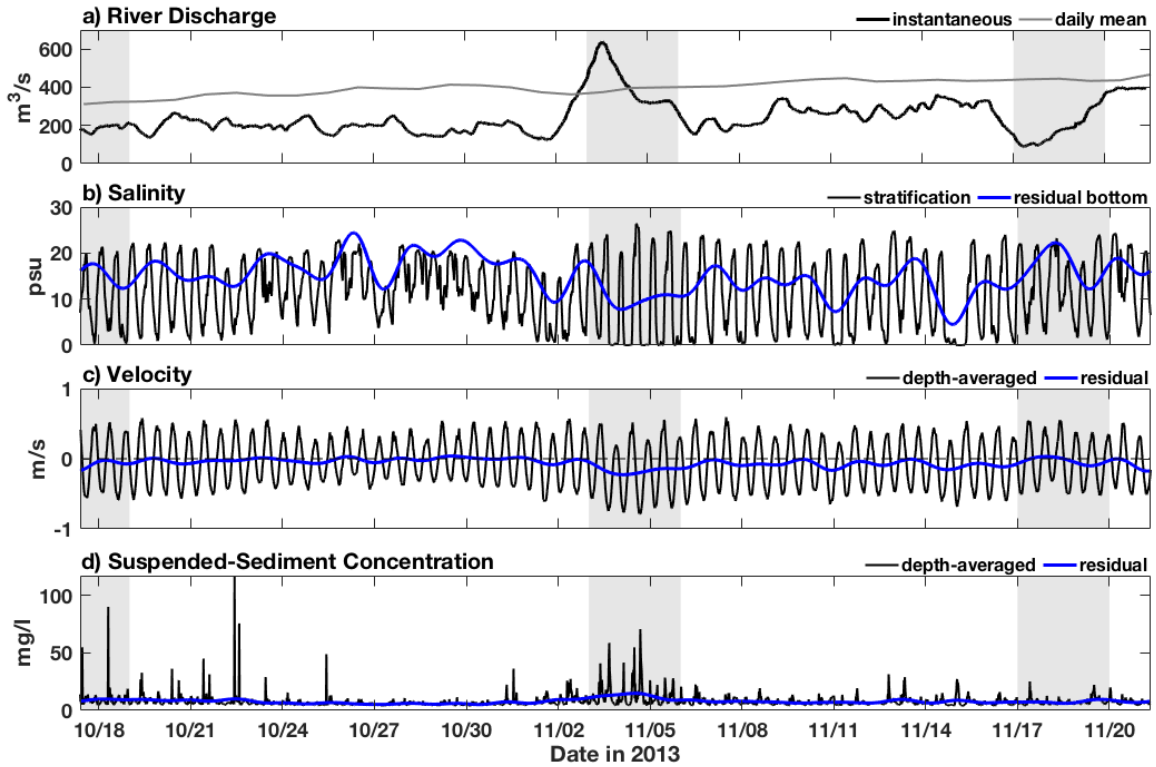
**Figure 3.** Calibrations for acoustic suspended-sediment data. **a)** Comparison of SSC derived from calibrated 5 MHz ABS backscatter to gravimetric SSC from colocated pumped water samples from 15 cm above the bed during a tidal cycle in Fall 2015. **b)** Comparison of SSC derived from calibrated and extrapolated ADCP backscatter to gravimetric SSC from colocated Niskin bottle water samples from ~0.5 m above the bed during a tidal cycle in Spring 2014. **c)** and **d)** Comparison of downward-looking 5 MHz ABS to upward-looking 1 MHz ABS at the same heights above the bed in the overlapping region of the two transducers (~0.5-0.9 m above bed) during Fall 2013 (c) and Fall 2015 (d); linear best-fit equations were used to calibrate the upward-looking 1 MHz data. The scatter in all regressions is attributed to different acoustic response to variable suspended-particle characteristics during different phases of the tide and river discharge conditions. Some of the scatter in (b) owes to slight differences in space and time of samples.



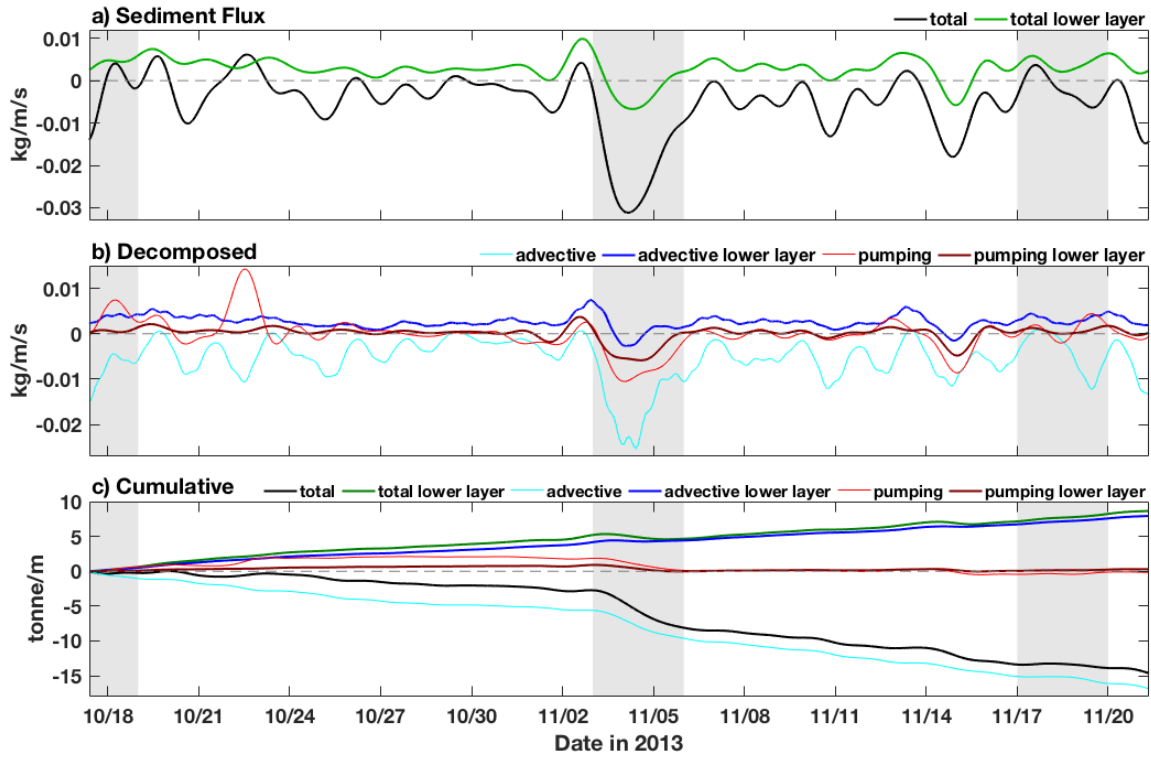
**Figure 4.** Connecticut River discharge (**a**) and SSC (**b**) from 2013 to 2015 including the three field deployments. SSC at Middle Haddam was calculated from an established rating curve (Yellen et al. 2014).



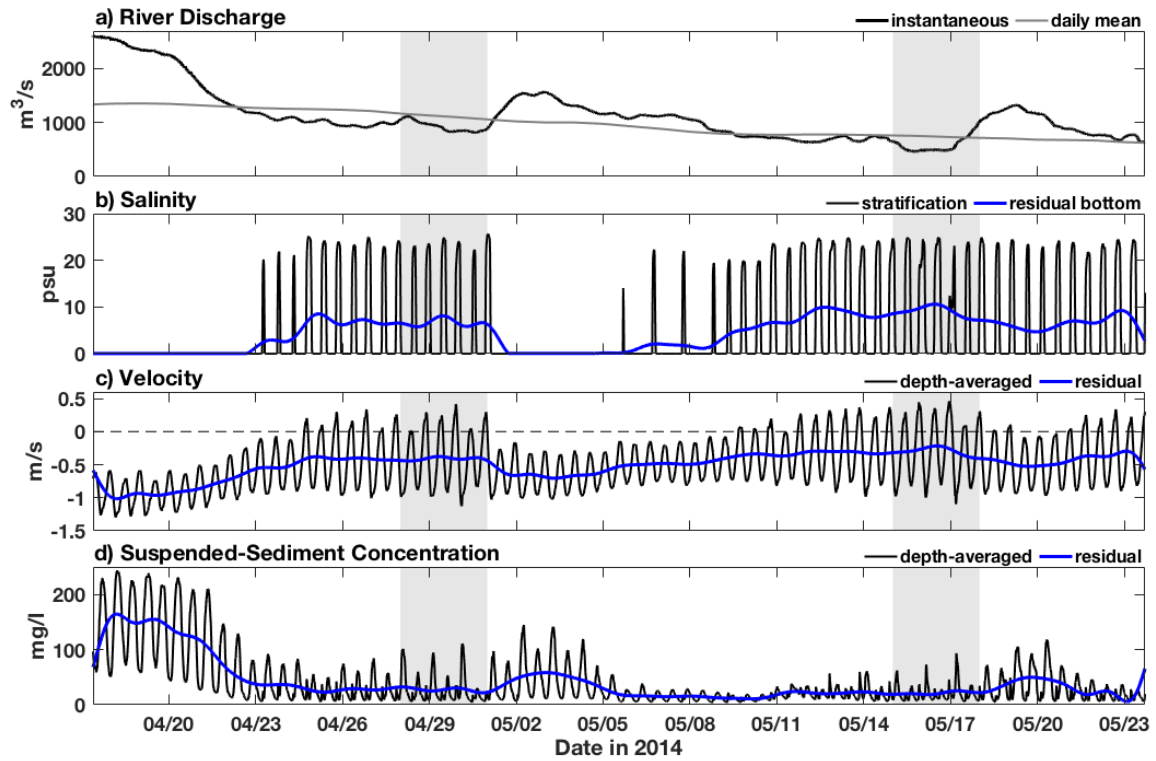
**Figure 5.** Mean profiles of velocity and SSC during Fall 2013 (a-b), Spring 2014 (c-d), and Fall 2015 (e-f). Solid bold lines represent mean profiles during times of maximum depth-averaged ebb current, dotted bold lines represent mean profiles during times of maximum depth-averaged flood current, and thin gray lines represent all profiles during maximum ebb and flood current from which the mean profiles were calculated (profiles during only below-mean discharge for Fall 2013 and Fall 2015, and all profiles for Spring 2014). Blue line segments represent extrapolated data. Positive velocities are up-estuary (landward). SSCs during Fall 2013 and Fall 2015 were obtained from calibrated ABS backscatter, and SSCs during Spring 2014 were obtained from calibrated ADCP backscatter. Note the different SSC scales.



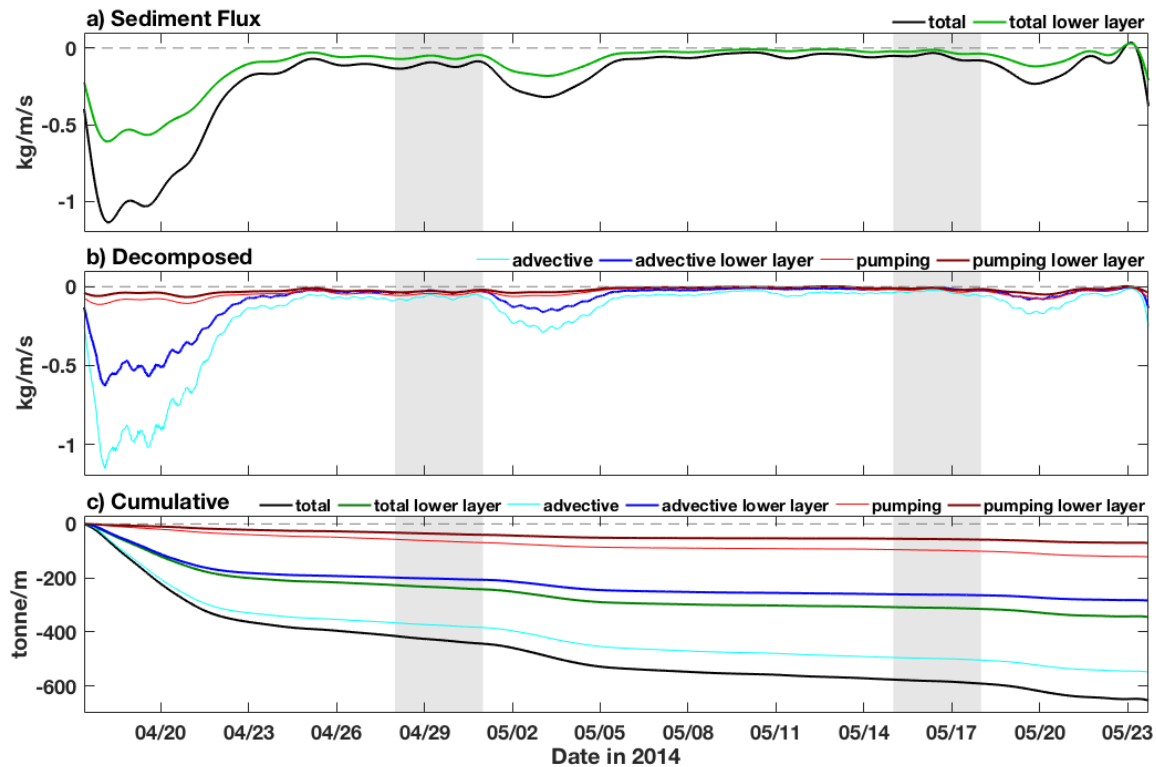
**Figure 6.** Time-series data collected during the Fall 2013 deployment in FZ4. **a)** Instantaneous and 88-year daily-mean river discharge at Thompsonville, CT. **b)** Salinity stratification (difference between bottom and surface salinity) and low-pass filtered (residual) bottom salinity. **c)** Depth-averaged and residual velocity, with positive values denoting up-estuary (landward) velocities. **d)** Depth-averaged and residual SSC. Gray shaded regions denote times of spring tides.



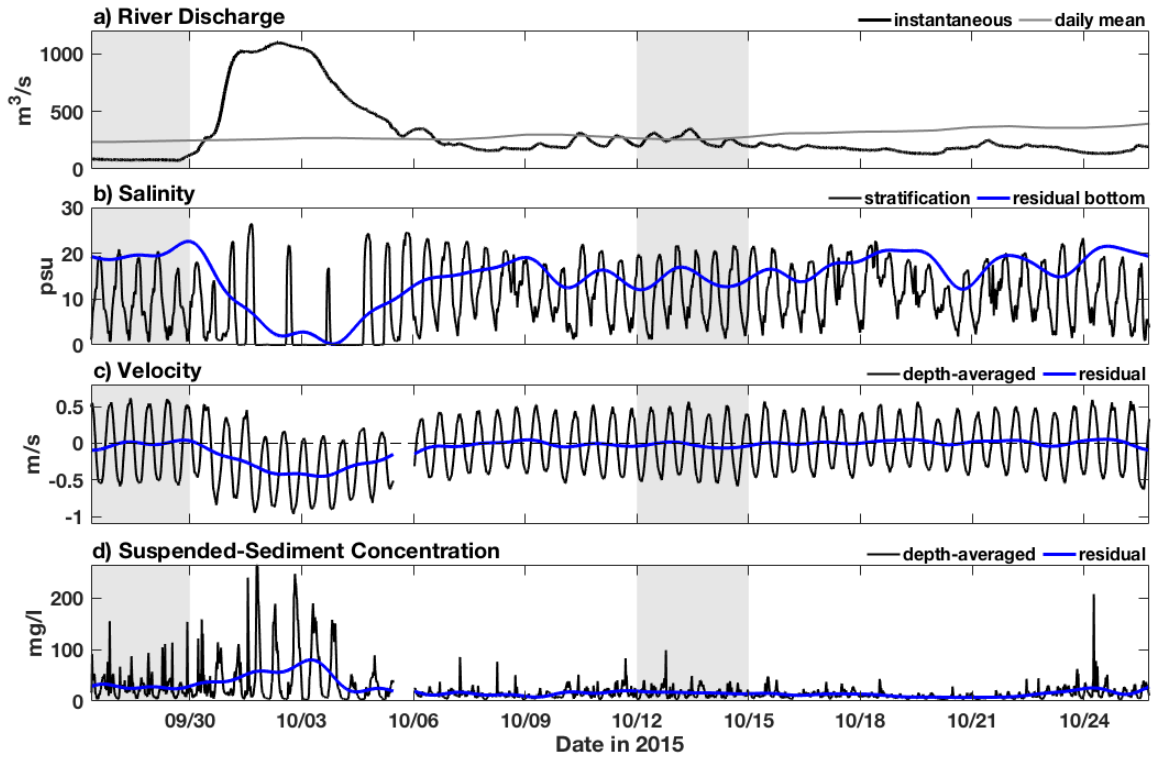
**Figure 7.** Time series of suspended-sediment fluxes during the Fall 2013 deployment in FZ4. **a)** Low-pass filtered (residual) total sediment flux integrated over the entire water column and over the lower layer (bottom 30% of the water column). **b)** Sediment flux decomposed into advective flux and tidal pumping flux, and integrated over the full water column and lower layer. **c)** Sediment fluxes from panels a-b accumulated over the deployment. Positive fluxes are up-estuary (landward). Gray shaded regions denote times of spring tides.



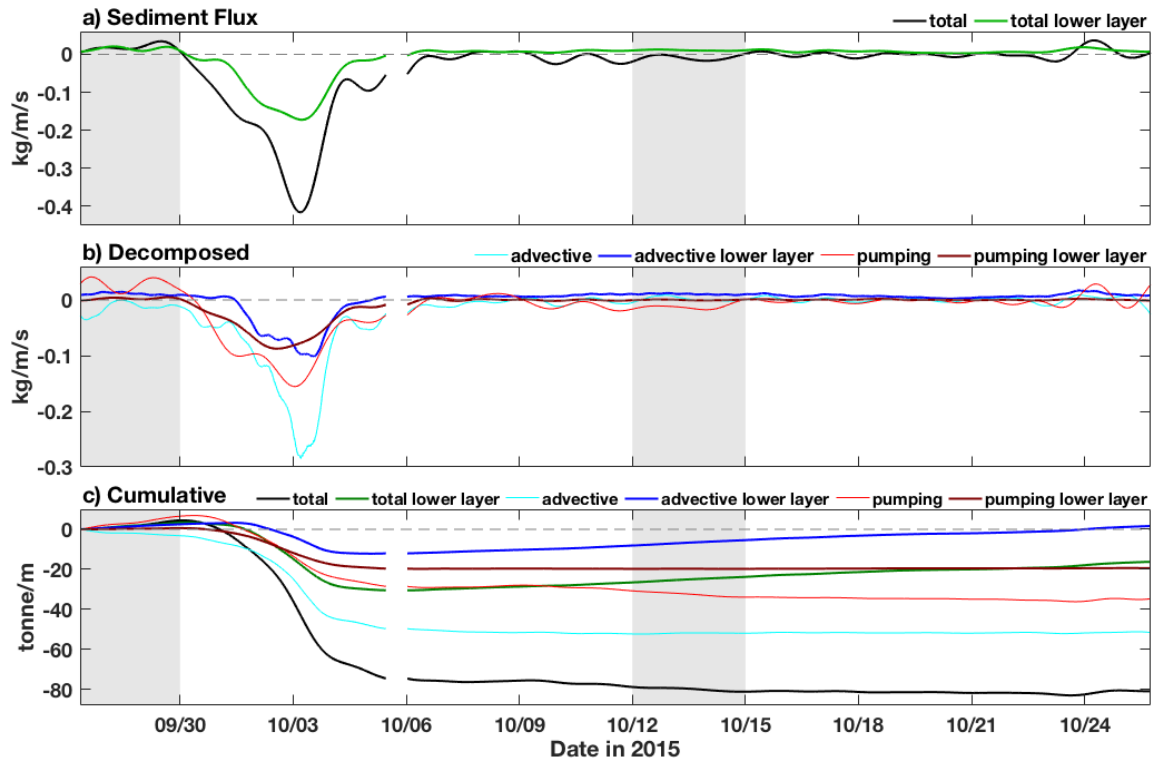
**Figure 8.** Time-series data collected during the Spring 2014 deployment in FZ3. **a)** Instantaneous and 88-year daily-mean river discharge at Thompsonville, CT. **b)** Salinity stratification (difference between bottom and surface salinity) and low-pass filtered (residual) bottom salinity. **c)** Depth-averaged and residual velocity, with positive values denoting up-estuary (landward) velocities. **d)** Depth-averaged and residual SSC. Gray shaded regions denote times of spring tides.



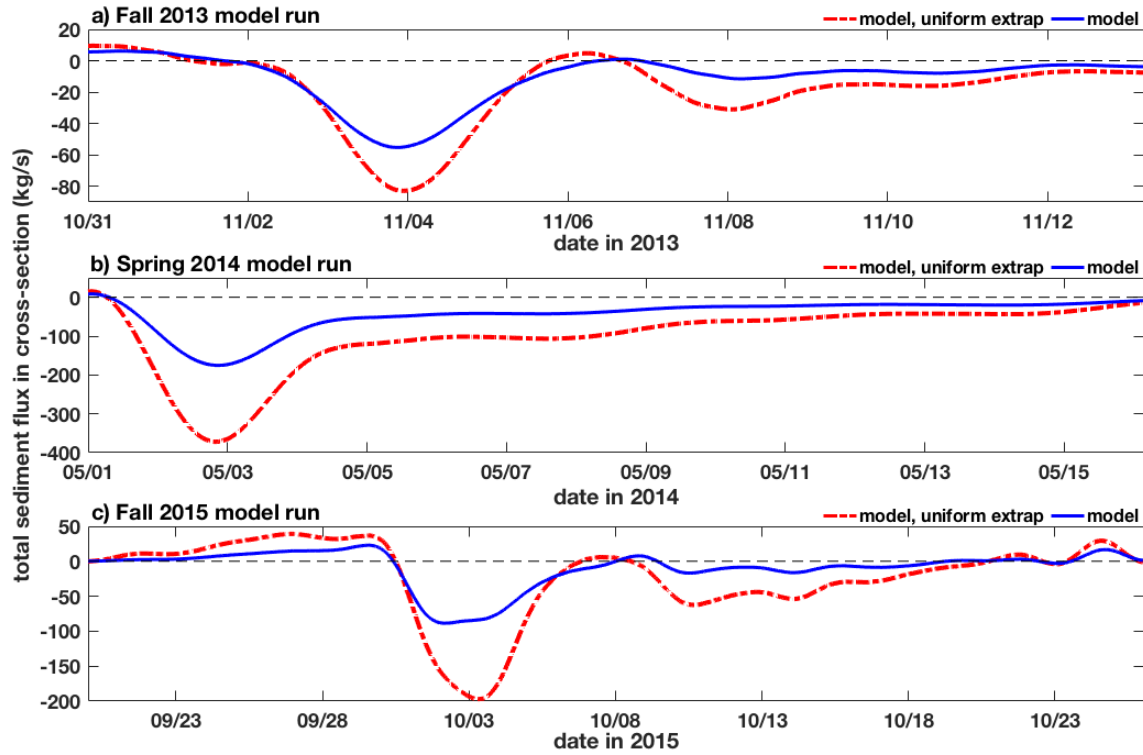
**Figure 9.** Time series of suspended-sediment fluxes during the Spring 2014 deployment in FZ3. **a)** Low-pass filtered (residual) total sediment flux integrated over the entire water column and over the lower layer (bottom 30% of the water column). **b)** Sediment flux decomposed into advective flux and tidal pumping flux, and integrated over the full water column and lower layer. **c)** Sediment fluxes from panels a-b accumulated over the deployment. Positive fluxes are up-estuary (landward). Gray shaded regions denote times of spring tides.



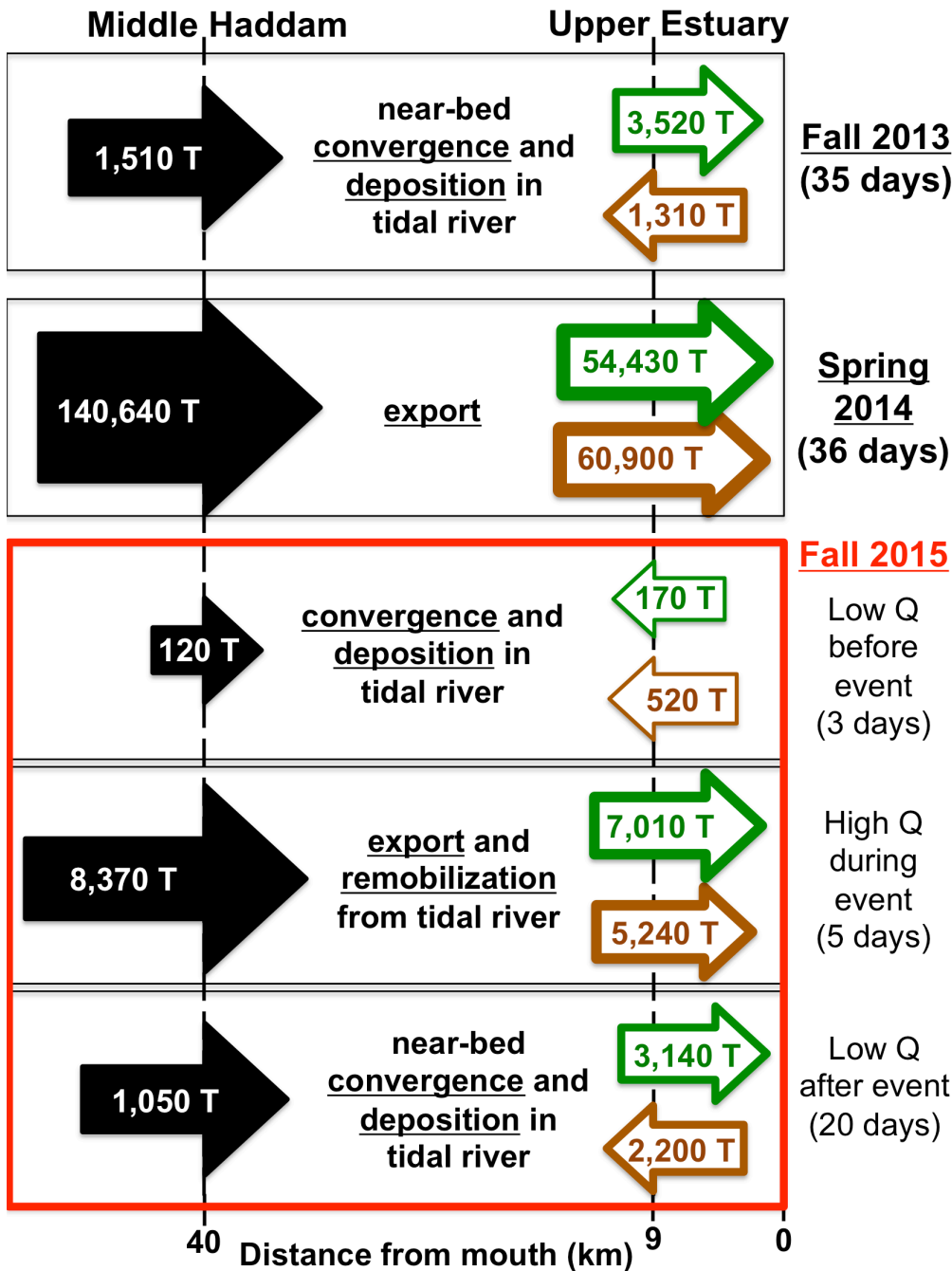
**Figure 10.** Time-series data collected during the Fall 2015 deployment in FZ4. **a)** Instantaneous and 88-year daily-mean river discharge at Thompsonville, CT. **b)** Salinity stratification (difference between bottom and surface salinity) and low-pass filtered (residual) bottom salinity. **c)** Depth-averaged and residual velocity, with positive values denoting up-estuary (landward) velocities. **d)** Depth-averaged and residual SSC. Gray shaded regions denote times of spring tides.



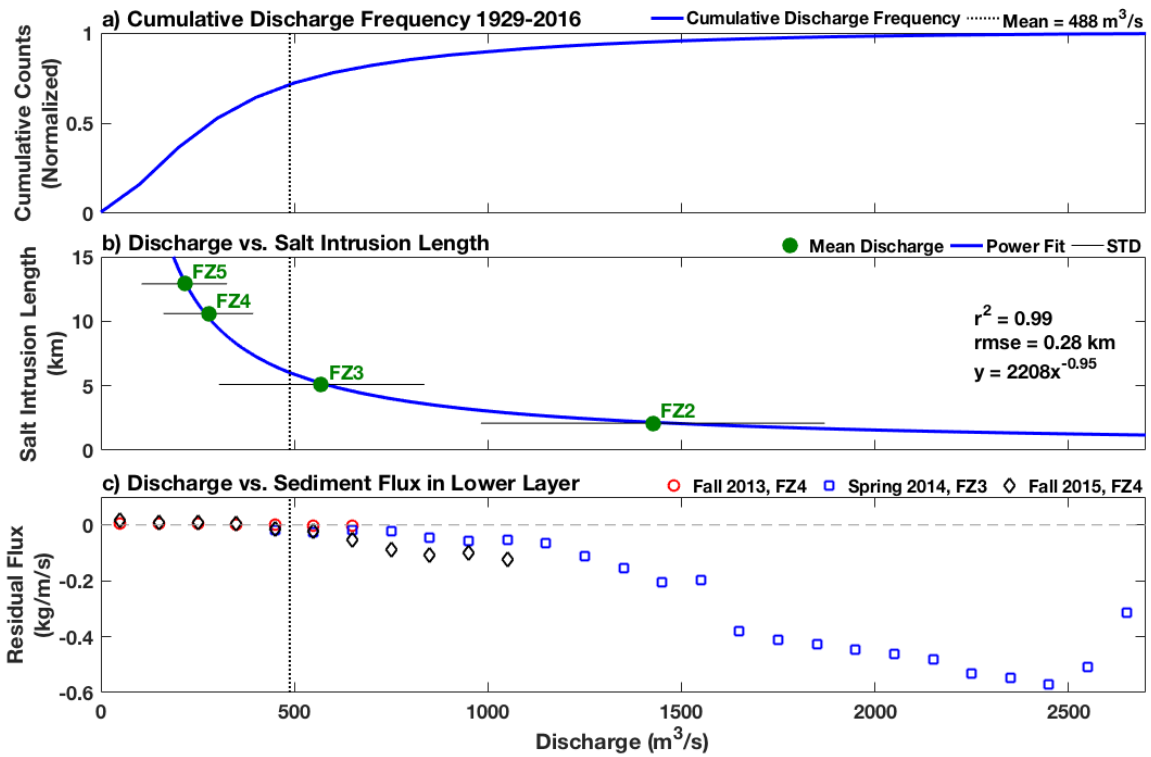
**Figure 11.** Time series of suspended-sediment fluxes during the Fall 2015 deployment in FZ4. **a)** Low-pass filtered (residual) total sediment flux integrated over the entire water column and over the lower layer (bottom 30% of the water column). **b)** Sediment flux decomposed into advective flux and tidal pumping flux, and integrated over the full water column and lower layer. **c)** Sediment fluxes from panels a-b accumulated over the deployment. Positive fluxes are up-estuary (landward). Gray shaded regions denote times of spring tides.



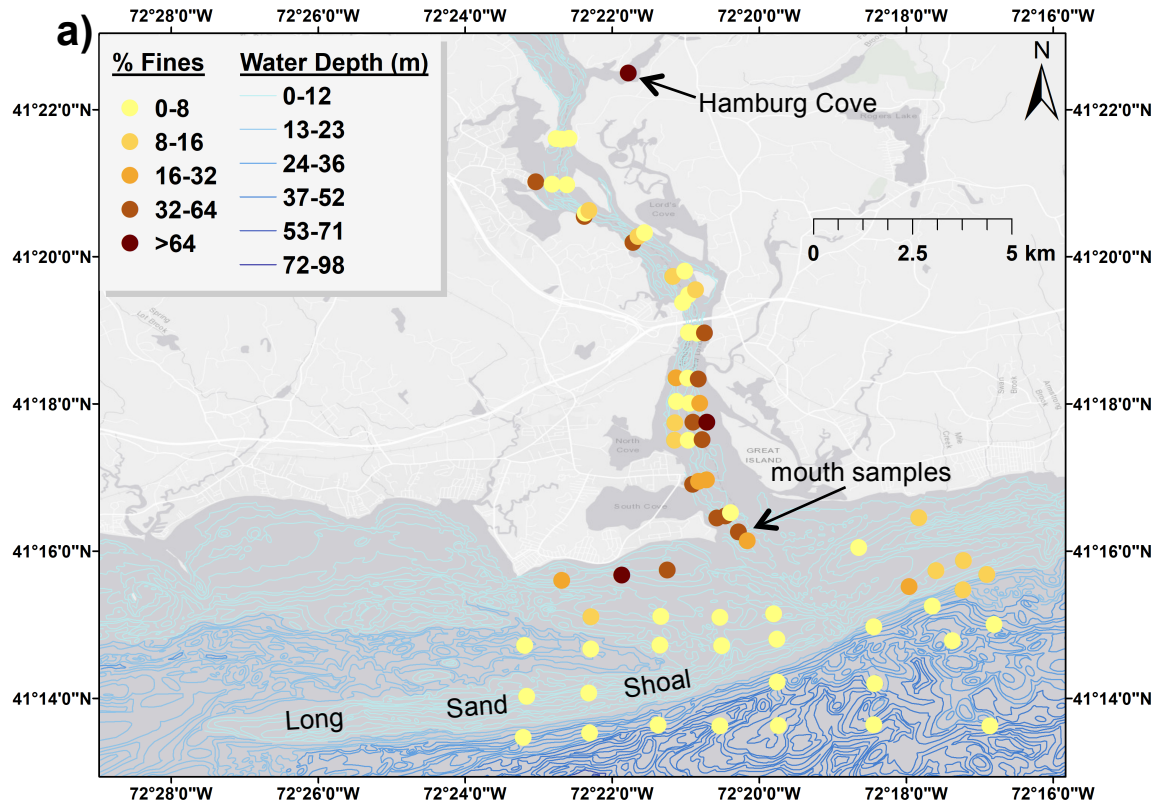
**Figure 12.** Model results of cross-channel integrated total sediment fluxes during the Fall 2013 (a), Spring 2014 (b) and Fall 2015 (c) deployment periods. Modeled fluxes are obtained from uniform extrapolation of the modeled flux in the thalweg, and from actual modeled fluxes integrated across the estuary. Uniform extrapolation overestimates the total flux by approximately a factor of two. Note the different y-axis scales for each panel.



**Figure 13.** Conceptual diagram illustrating total cross-section integrated sediment fluxes during all three field seasons, with Fall 2015 separated into three distinct periods based on changes in river discharge (red box). Black arrows represent fluxes past Middle Haddam in the tidal river (40 km from mouth), green arrows represent fluxes in the upper 70% of the water column in the estuary, and brown arrows represent fluxes in the lower 30% of the water column in the estuary (lower layer). Estuary fluxes during Fall 2013 and Fall 2015 are from FZ4 (9 km from mouth) and fluxes during Spring 2014 are from FZ3 (6 km from mouth). Fluxes correspond to model-guided values reported in Table 4.

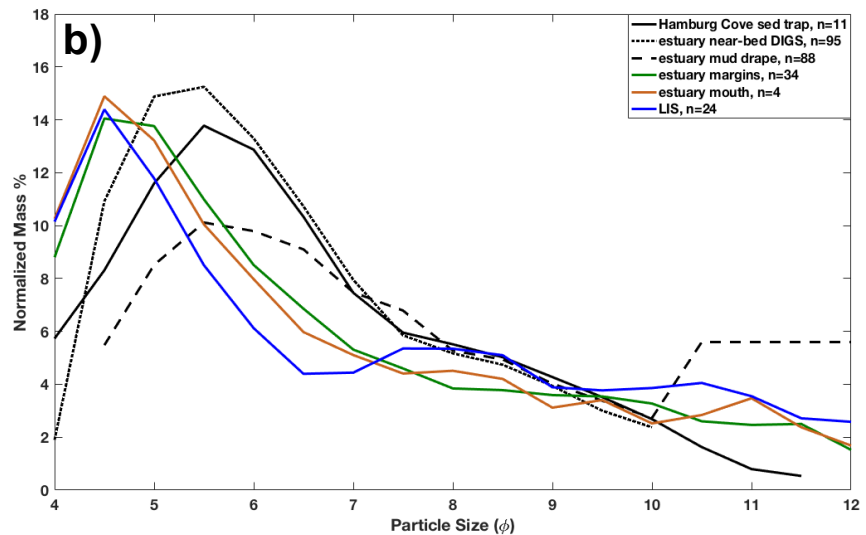


**Figure 14.** Effects of river discharge on salt intrusion length and sediment flux. **a)** Cumulative frequency distribution for all discharge data measured at Thompsonville, CT (USGS gauge #01184000) from 1929-2016. The x-axis has been truncated to only include discharge values observed during this study (the largest recorded discharge is  $7872 \text{ m}^3/\text{s}$ ), and only 0.3% of recorded values exceed this range. **b)** Inverse power-law relationship between discharge and salt intrusion length, defined by the maximum upstream distance where salinity was detected above 2 psu during each tidal cycle, as constrained by the four long-term moored CTDs. **c)** Relationship between discharge and residual sediment flux in the lower layer from all three field deployments. Landward (positive) fluxes are observed for discharges below  $\sim 400 \text{ m}^3/\text{s}$ .



**Figure 15. a)** Map of the Connecticut River estuary and northeastern Long Island Sound (LIS) showing the percent of fine sediments ( $>4 \phi$  or  $<63 \mu\text{m}$ ) at each sampling location. Blue lines are bathymetry, and notable features are labeled. Hamburg Cove grain-size data

are from Yellen et al. (2017), estuary data are modified from Valentine (2015) and Lavallee (2017), and LIS data are from this study. **b)** Mean normalized grain-size distributions of fine sediments from sediment traps inside Hamburg Cove, near-bed suspended samples, mud drape sediment, and bed sediment from the estuary margins, estuary mouth and LIS. All grain-size distributions are unimodal with modes of  $4.5 \phi$  for the bed samples and  $5.5 \phi$  for the recently-suspended samples. Legend includes the number of individual distributions for each sample type that were averaged. The mud drape distribution (dashed black line) ended with a large value at  $10.5 \phi$  which was equally divided over the range  $10.5-12 \phi$ .



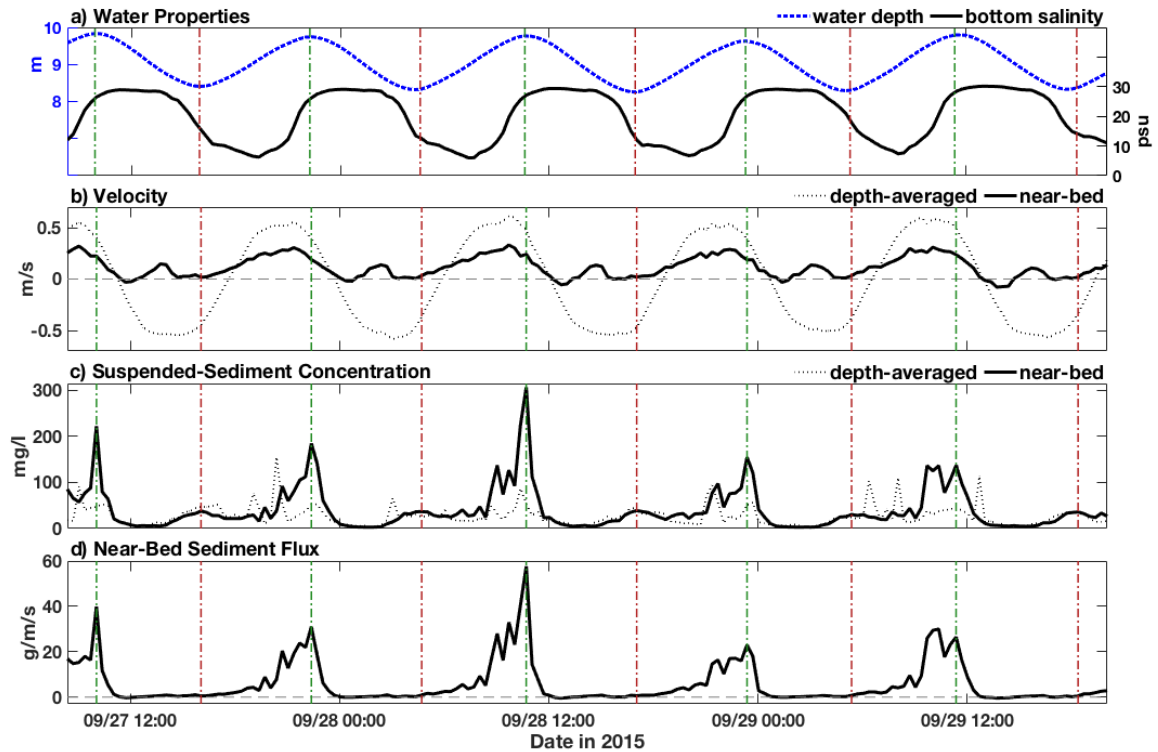


**Figure 16.** Zoom-in of time-series data during low discharge at the beginning of the Fall 2015 deployment in FZ4, illustrating the role of the advancing salt intrusion in transporting sediment landward. **a)** Water depth and bottom salinity. **b)** Depth-averaged and near-bed velocity. **c)** Depth-averaged and near-bed SSC. **d)** Near-bed suspended-sediment flux. Positive values of velocity and flux are up-estuary (landward). Vertical dashed lines denote the times of peak near-bed SSC during the flood tide (green) and ebb tide (red).

## 8.0 REFERENCES

- Ackerman, S.D., Foster, D.S., Moore, E.M., Irwin, B.J., Blackwood, D., and Sherwood, C.R., 2017, High-resolution geophysical and sampling data collected at the mouth of Connecticut River, Old Saybrook to Essex, Connecticut, 2012, USGS Field Activity 2012-024-FA: U.S. Geological Survey data release. <https://doi.org/10.5066/F7PG1Q7V>
- Betteridge, K.F.E., Thorne, P.D., and R.D. Cooke. 2008. Calibrating multi-frequency acoustic backscatter systems for studying near-bed suspended sediment transport processes. *Cont Shelf Res* 28(2):227–235.
- Burchard, H., Schuttelaars, H.M., and D.K. Ralston. 2018. Sediment trapping in estuaries. *Annu Rev Mar Sci* 10(14):1–25.
- Castaing, P., and G.P. Allen. 1981. Mechanisms controlling seaward escape of suspended sediment from the Gironde: A macrotidal estuary in France. *Mar Geol* 40:101–118.
- Chen, C., Liu, H., and R.C. Beardsley. 2003. An unstructured grid, finite-volume, three-dimensional, primitive equations ocean model: Application to coastal ocean and estuaries. *J Atmospheric Ocean Technol* 20(1):159–186.
- Cook, T.L., Sommerfield, C.K., and K.-C. Wong. 2007. Observations of tidal and springtime sediment transport in the upper Delaware Estuary. *Estuar Coast Shelf S* 72:235–246.
- Downing, A., Thorne, P.D., and C.E. Vincent. 1995. Backscattering from a suspension in the near field of a piston transducer. *J Acoust Soc Am* 97(3):1614–1620.
- Festa, J.F., and D.V. Hansen. 1978. Turbidity maxima in partially mixed estuaries: a two-dimensional numerical model. *Estuar Coast Mar Sci* 7(4):347–359.
- Folk, R.L., and W.C. Ward. 1957. Brazos River bar: a study in the significance of grain size parameters. *J Sediment Petrol* 27(1):3–26.
- Ganju, N.K., and D.H. Schoellhamer. 2009. Calibration of an estuarine sediment transport model to sediment fluxes as an intermediate step for simulation of geomorphic evolution. *Cont Shelf Res* 29:148–158.
- Gartner, J.W. 2004. Estimating suspended solids concentrations from backscatter intensity measured by acoustic Doppler current profiler in San Francisco Bay, California. *Mar Geol* 211:169–187.
- Garvine, R.W. 1974. Physical features of the Connecticut River outflow during high discharge. *J Geophys Res* 79(6):831-846.

- Garvine, R.W. 1975. The distribution of salinity and temperature in the Connecticut River estuary. *J Geophys Res* 80(9):1176–1183.
- Geyer, W.R. 1993. The importance of suppression of turbulence by stratification on the estuarine turbidity maximum. *Estuaries* 16(1):113–125.
- Geyer, W.R. 2010. Estuarine salinity structure and circulation. In: Valle-Levinson A, editor. *Contemporary issues in estuarine physics*. Cambridge: Cambridge University Press. p. 12-26.
- Geyer, W.R., and D.M. Farmer. 1989. Tide-induced variation of the dynamics of a salt wedge estuary. *J Phys Oceanogr* 19(8):1060–1072.
- Geyer, W.R., and P. MacCready. 2014. The estuarine circulation. *Annu Rev Fluid Mech* 46(1):175–197.
- Geyer, W.R., and D.K. Ralston. 2015. Estuarine frontogenesis. *J Phys Oceanogr* 45:546–561.
- Geyer, W.R., and D.K. Ralston. 2018. A mobile pool of contaminated sediment in the Penobscot Estuary, Maine, USA. *Sci Total Environ* 612:694–707.
- Geyer, W.R., Woodruff, J., and P. Traykovski. 2001. Sediment transport and trapping in the Hudson River estuary. *Estuaries* 24(5):670–679.
- Geyer, W.R., Lavery, A.C., Scully, M.E., and J.H. Trowbridge. 2010. Mixing by shear instability at high Reynolds number. *Geophys Res Lett* 37(L22607):1–5.
- Grabemann, I., and G. Krause. 1989. Transport processes of suspended matter derived from time series in a tidal estuary. *J Geophys Res* 94(C10):14373–14379.
- Holleman, R.C., Geyer, W.R., and D.K. Ralston. 2016. Stratified turbulence and mixing efficiency in a salt wedge estuary. *J Phys Oceanogr* 46(6):1769–1783.
- Hong, B., and J. Shen. 2012. Responses of estuarine salinity and transport processes to potential future sea-level rise in the Chesapeake Bay. *Estuar Coast Shelf S* 104–105:33–45.
- Horne, G.S., and P.C. Patton. 1989. Bedload-sediment transport through the Connecticut River estuary. *Geol Soc Am Bull* 101:805–819.
- Jay, D.A., and J.D. Musiak. 1994. Particle trapping in estuarine tidal flows: *J Geophys Res* 99(C10):20,445–20,461.

- Lavallee, K.D. 2017. Suspended cohesive particle characteristics in the Connecticut River estuary. M.S. thesis, Boston College, Boston, MA. 91 p.
- Lemieux, C.R. 1983. Suspended sediment transport in the Connecticut River estuary. B.S. thesis, Wesleyan University, Middletown, CT. 117 p.
- Lerczak, J.A., Geyer, W.R., and D.K. Ralston. 2009. The temporal response of the length of a partially stratified estuary to changes in river flow and tidal amplitude. *J Phys Oceanogr* 39(4):915–933.
- Liu, S., Shi, X., Liu, Y., Zhu, Z., Yang, G., Zhu, A., and J. Gao. 2011. Concentration distribution and assessment of heavy metals in sediments of mud area from inner continental shelf of the East China Sea. *Environ Earth Sci* 64(2):567–579.
- Lynch, J.F., Gross, T.F., Sherwood, C.R., Irish, J.D., and B.H. Brumley. 1997. Acoustical and optical backscatter measurements of sediment transport in the 1988-1989 STRESS experiment. *Cont Shelf Res* 17(4):337–366.
- Meade, R.H. 1969. Landward transport of bottom sediments in estuaries of the Atlantic coastal plain. *J Sediment Petrol* 39(1):222–234.
- Medwin, H., and C.S. Clay. 1998. *Fundamentals of acoustical oceanography*. Boston, Academic Press, 712 p.
- Menon, M.G., Gibbs, R.J., and A. Phillips. 1998. Accumulation of muds and metals in the Hudson River estuary turbidity maximum. *Environ Geol* 34(2/3):214–222.
- Milligan, T.G., Kineke, G.C., Blake, A.C., Alexander, C.R., and P.S. Hill. 2001. Flocculation and sedimentation in the ACE Basin, South Carolina. *Estuaries* 24(5):734–744.
- Patton, P.C., and G.S. Horne. 1992. Response of the Connecticut River estuary to late Holocene sea level rise. *Geomorphology* 5:391–417.
- Poppe, L.J., Knebel, H.J., Lewis, R.S., and M.L. DiGiacomo-Cohen. 2002. Processes controlling the remobilization of surficial sediment and formation of sedimentary furrows in north-central Long Island Sound. *J Coastal Res* 18(4):741–750.
- Ralston, D.K., and W.R. Geyer. 2017. Sediment transport time scales and trapping efficiency in a tidal river. *J Geophys Res-Earth* 122:1–22.
- Ralston, D.K., Geyer, W.R., and J.A. Lerczak. 2010. Structure, variability, and salt flux in a strongly forced salt wedge estuary. *J Geophys Res* 115(C06005):1–21.

- Ralston, D.K., Geyer, W.R., and J.C. Warner. 2012. Bathymetric controls on sediment transport in the Hudson River estuary: lateral asymmetry and frontal trapping. *J Geophys Res* 117(C10013): 1–21.
- Ralston, D.K., Geyer, W.R., Traykovski, P., and N.J. Nidzioko. 2013. Effects of estuarine and fluvial processes on sediment transport over deltaic tidal flats. *Cont Shelf Res* 60S:S40–S57.
- Ralston, D.K., Cowles, G.W., Geyer, W.R., and R.C. Holleman. 2017. Turbulent and numerical mixing in a salt wedge estuary: dependence on grid resolution, bottom roughness, and turbulence closure. *J Geophys Res-Oceans* 122:1–21.
- Rouse, H. 1937. Modern conceptions of the mechanics of fluid turbulence. *T Am Soc Civ Eng* 102(1):463–541.
- Scatena, F.N. 1982. Patterns of bedload transport in the Connecticut River estuary. M.A. thesis, Wesleyan University, Middletown, CT. 124 p.
- Schubel, J.R. 1968. Turbidity maximum of the Northern Chesapeake Bay. *Science* 161(3845):1013–1015.
- Scully, M.E., and C.T. Friedrichs. 2003. The influence of asymmetries in overlying stratification on near-bed turbulence and sediment suspension in a partially mixed estuary. *Ocean Dynamics* 53(3):208–219.
- Scully, M.E., and C.T. Friedrichs. 2007. Sediment pumping by tidal asymmetry in a partially mixed estuary. *J Geophys Res* 112:C07028.
- Signell, R.P., List, J.H., and A.S. Farris. 2000. Bottom currents and sediment transport in Long Island Sound: a modeling study. *J Coastal Res* 16(3):551–566.
- Simmons, H.B., and F.A. Herrmann Jr. 1972. Effects of man-made works on the hydraulic, salinity, and shoaling regimens of estuaries. *Geol Soc Am Mem* 133:555–570.
- Sommerfield, C.K., and K.-C. Wong. 2011. Mechanisms of sediment flux and turbidity maintenance in the Delaware Estuary. *J Geophys Res* 116(C01005):1–16.
- Sternberg, R.W., Kineke, G.C., and R. Johnson. 1991. An instrument system for profiling suspended sediment, fluid, and flow conditions in shallow marine environments. *Cont Shelf Res* 11(2): 109–122.
- Temmerman, S., Govers, G., Wartel, S., and P. Meire. 2004. Modeling estuarine variations in tidal marsh sedimentation: response to changing sea level and suspended sediment concentrations. *Marine Geology* 212(1–4):1–19.

- Thorne, P.D., Hardcastle, P.J., and R.L. Soulsby. 1993. Analysis of acoustic measurements of suspended sediments. *J Geophys Res* 98(C1):899–910.
- Thorne, P.D., and P.J. Hardcastle. 1997. Acoustic measurements of suspended sediments in turbulent currents and comparison with in-situ samples. *J Acoust Soc Am* 101(5):2603–2614.
- Thorne, P.D., and D.M. Hanes. 2002. A review of acoustic measurement of small-scale sediment processes. *Cont Shelf Res* 22(4):603–632.
- Thorne, P.D., and D. Hurther. 2014. An overview on the use of backscattered sound for measuring suspended particle size and concentration profiles in non-cohesive inorganic sediment transport studies. *Cont Shelf Res* 73:97–118.
- Toney, J.D. 1987. Historical sediment storage and pollen stratigraphy of the lower Connecticut River estuary. M.A. thesis, Wesleyan University, Middletown, CT. 112 p.
- Traykovski, P., Geyer, W.R., and C. Sommerfield. 2004. Rapid sediment deposition and fine-scale strata formation in the Hudson estuary. *J Geophys Res* 109(F02004): 1–20.
- United States Geological Survey. 2015. [waterdata.usgs.gov](http://waterdata.usgs.gov).
- Valentine, K. 2015. Characterization of the bed, critical boundary shear stress, roughness, and bedload transport in the Connecticut River estuary. M.S. thesis, Boston College, Boston, MA. 144 p.
- Valle-Levinson, A., and C.A.F. Schettini. 2016. Fortnightly switching of residual flow drivers in a tropical semiarid estuary. *Estuar Coast Shelf S* 169:46–55.
- Warner, J.C., Sherwood, C.R., Signell, R.P., Harris, C.K., and H.G. Arango. 2008. Development of a three-dimensional, regional, coupled wave, current, and sediment-transport model. *Comput Geosci* 34(10):1284–1306.
- Wehof, J. 2015. Instrumentation to measure suspended sediment in a stratified estuary. General Exam Part 2, Written Report, Woods Hole Oceanogr. Inst., Woods Hole, Mass.
- Wellershaus, S. 1981. Turbidity maximum and mud shoaling in the Weser estuary. *Arch Hydrobiol* 92:161–198.
- Woodruff, J.D., Martini, A.P., Elzidani, E.Z.H., Naughton, T.J., Kekacs, D.J., and D.G. Macdonald. 2013. Off-river waterbodies on tidal rivers: human impact on rates of infilling and the accumulation of pollutants. *Geomorphology* 184:38–50.

- Yellen, B., Woodruff, J.D., Kratz, L.N., Mabee, S.B., Morrison, J., and A.M. Martini. 2014. Source, conveyance and fate of suspended sediments following Hurricane Irene. New England, USA. *Geomorphology* 226:124–134.
- Yellen, B., Woodruff, J.D., Ralston, D.K., MacDonald, D.G., and D.S. Jones. 2017. Salt wedge dynamics lead to enhanced sediment trapping within side-embayments in high-energy estuaries. *J Geophys Res-Oceans* 122(3):2226–2242.